Source details

NeuroQuantology

Scopus coverage years: from 2007 to 2022

Publisher: Anka Publishers

ISSN: 1303-5150

Subject area: (Physics and Astronomy: Atomic and Molecular Physics, and Optics) (Neuroscience: Cognitive Neuroscience)

(Neuroscience: Developmental Neuroscience)

Source type: Journal

☐ Save to source list   Source Homepage

CiteScore   CiteScore rank & trend   Scopus content coverage

CiteScore 2021
1.3

SJR 2021
0.285

SNIP 2021
1.038

About Scopus

What is Scopus
Content coverage
Scopus blog
Scopus API
Privacy matters

Language

日本語に切り替える
切换到简体中文
切換到繁體中文
Просмотр версии на русском языке

Customer Service

Help
Tutorials
Contact us

IQAC In-charge
Rajiv Gandhi College of Engineering
Karjule Harya, Tal. Parner
Dist. Ahmednagar-414304

Principal
R G COE, Karjule Harya.

Performance Investigation on Solar Dryer Using Flat Plate Collector

Dr. Krupal Pawar[1*], Bhusan Dusane[2]
Associate Professor, Mechanical Engg. Department, Rajiv Gandhi College of Engineering, Karjule Harya[1]
Assistant Professor, Mechanical Engg. Department, Sandip University, Nashik[2]
Email:krupalpawar@gmail.com

Abstract

Solar Drying is one of the important processes required for the preservation of food and agricultural products. Bacterial growth and moisture are removed in this process. It helps for preserving the food products for more long time. Solar drying is an effective method used for drying food products. The device used to preserve food products using solar energy is called a solar dryer or solar dehydrator. The solar dryer is classified based on the drying mode, air circulation, type, and arrangement of a cabinet of solar air collectors. The preserved raisin is a favorite dry fruit in India. Traditionally the drying of raisins mainly exposes natural sunlight and requires about 21 days. This experiment used a comparative study between natural sun drying and solar drying using a flat-plated collector dryer from 29th March 2020 to 19th April 2020. The incident area of solar radiation on the collector was 0.9m², with a black rough surface aluminum plated absorber of 1.8m² attached below the covered acrylic glazing used in the collector body. It was found that the latitude inclination of 19.5° had a maximum temperature of 69°C during 01:00 PM – 02.00 PM hours. The result found that drying raisins naturally takes up to 21 days, and comparatively, it takes 7 days to dry using the solar dryer. Thus, the drying period is reduced by 14 days.

Key Words: Solar Drying, Raisins, Agriculture Products, Natural Sunlight.

I. INRODUCTION

The drying of grapes to form into raisins usually relies on direct sunlight exposure. This drying method requires more periods and lower quality of dried products. Drying of grapes is usually conducted under low temperatures, and thus, the use of solar dryers for dehydrating grapes is one of the best alternatives. Due to energy crises, most of the food processing and food preservation activities in the industries are depends upon non-renewable energy sources. It needs to check for alternatives for non-renewable and polluting fossil fuels. The use of renewable energy sources like solar energy is one of the best solutions for reducing the usage of non-renewable sources. The sun produces its energy through many thermonuclear reactions which create a large amount of heat and electromagnetic radiation which is easily available throughout the earth. This solar energy is trapped by heat exchanger devices called solar collectors. By comparing solar drying with traditional drying, solar drying has advantages such as better quality of food products, reduction in wastage of food products, a better market price can be achieved the product can be protected against flies, rain, and dust, the product can be left in the dryer overnight during rain, since dryers are waterproof, prevent fuel dependence and reduces the environmental impact, it is more efficient and cheaper [7].

The chosen raw material was grapes, which is a versatile spring crop. We kept 500 grams of grapes in the tray for the initial experiment. Grapes required drying temperatures ranging from 20°C to 60°C. The reason behind the selection of grapes as a raw material is the prices of dried grapes or raisins is much higher than the prices of fresh grapes available in the market, also per 100 gram of fresh grapes contains 81% of the water in it and the nutrition value we get is, 18% carbohydrates, 1% protein, 69Kcal energy and a moderate amount of vitamin K (14% of daily value) which can get from only 29 gram of split dried raisins (dried grapes), according to USDA (US department of agriculture) [1-3]. The effect of environmental conditions plays a vital role in the performance of solar dryers. The minimum temperature required to use the solar dryer system for processing food is 15°C [1]. The performance is affected by the use of material quality such as Aluminium sheets at the inner side give better results in drying foods. It also acts as a good absorber [2]. The parameters that decide the results are moisture, solar radiation, wind speed, and humidity. The addition of a fan/blower to introduce indirect forced convection will help to enhance performance as well as reduce heat loss during the operation [9]. The flow of air at the inner side may be unidirectional or bidirectional which is generally affected by external air wind speed [8]. While the shape and geometry of collectors are the research area in which work can be tested by changing parameters. However, the performance of solar dryers varies around 10-15% in terms of efficiency and the general achieved temperature range is 50+°C with 15-22% of Relative Humidity [11].

II. EXPERIMENTAL SETUP

The experimental model consists of major components like a flat plate collector and drying chamber which are connected by the flexible pipe for the transfer of drying high-temperature air from the collector to the drying chamber. A flat plate collector is designed as per a multi-stage pattern to achieve more heat and it consists of layers of insulator and absorber in it, which are air securely covered by an acrylic sheet to convey solar radiation to the absorber. The

1420

drying chamber cabinet is isolated with insulator material and contains two trays of size 600 mm X 600 mm for carrying the food hub for drying. For measurement purposes Arduino based smart data logging system is used which contains DHT22 & DHT11 respectively temperature and humidity sensors have a range of Temperature -40°C to 100°C and humidity 0% to 100% which are further connected with Arduino UNO motherboard and 16 X 2 character Alphanumerical display for showing the temperature and humidity values of sensors which kept in locations of a setup like Temperature & humidity at ambient, Temperature & humidity at absorber surface of collector, Temperature & humidity of air exhaled from the collector, Temperature & humidity inside the drying chamber[1-3]. The RTC (Real-time clock) device is used to indicate and manipulate the temperature and humidity data concerning time. The SD card logger is used to store the daily data of temperatures and humidity at different conditions. The model is programmed as per auto ON & OFF of the system from 10.00 AM to 06.00 PM. This study is conducted to examine the thermal characteristics of the solar dryer with a flat-plated collector.

1421

A. Flat-plated Solar Air Collector

The flat plate solar air collector consists of components like a layer of insulation material, charcoal black painted absorber plates, airflow passages, acrylic glass, and coating material.
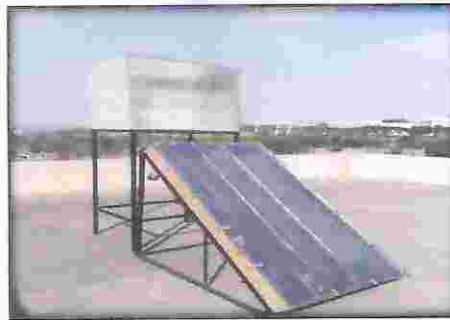

Fig.1 Flat-plated Solar Air Collector

Fig.2 Solar Collector with Absorber Surface

The cabinet body of the flat plate solar collector is made up of wooden plywood of inner sizes of 1500 mm X 600 mm X 120 mm and has a thickness of 12MM.the material for insulation of the collector body is polystyrene foam sheets and Aluminum foil having lower thermal conductivities of 0.033 W/mK & 0.06 W/mK respectively used to reduce the heat loss.

Fig.3 Solar air collector insulation

IQAC In-charge
Rajiv Gandhi College of Engineering
Karjule Harya, Tal. Parner
Dist. Ahmednagar-414304

www.neuroquantology.com

Principal
R.G.C.O.E. Karjule Harya,

1422

Fig.4 Complete Experimental Assembly of Setup

The absorber element used for absorbing solar radiation is the rough texture of an aluminum sheet of 0.5 mm thickness in a conical harmonic shape for providing more surface area for absorber plates. These absorber plates are painted black with charcoal-activated paint. The important material used in the collector body is the acrylic glass sheet of thickness 3 mm. The solar collector is mounted and supported on a heavy-duty mild steel structure which is durable and adjustable concerning latitude angle and can be set up into standard angles like 15°, 20°, 35°, 40°, and 45° as per investigation performance at different latitude angles.

B. Drying Chamber

The drying chamber cabinet is constructed from wooden plywood material to reduce heat losses. The dimensions of the drying chamber are 600 mm X 600 mm X 600 mm with a thickness of 12 mm. The drying chamber is insulated by a polystyrene foam sheet and aluminum foil from the interior to reduce heat losses. Two trays made up of meshed steel structures are used inside the drying chamber to contain food products for the drying process. Both trays are placed at 250 mm distinct from each other. The drying chamber is constructed with a chimney at the top for sweeping out humid air from the drying chamber. The collector and the drying chamber are connected utilizing a flexible pipe of diameter 2 inches.

C. Fans (Air Exhauster)

At the end of each stage, a pair of DC fans are used in solar collectors with a discharge of 35 CFM and a total power rating of 12V 0.18 W for each fan. The velocity of air can be controlled with the help of a DC regulator.

III. METHODOLOGY

The performance investigation is carried out in two experimental procedures. In the first experiment, an amount of 500-gram fresh grapes were kept directly in an open atmosphere for drying. This study is based on a daily record of the amount of weight drop and change in color of the grape converting into perfect raisins. The second experimental project model of a solar dryer which consists of a flat-plated multi-stage air flowing collector and drying cabinet chamber is tested by using a measured number of fresh grapes of 500 grams which were kept in the solar dryer for testing and investigation of weight drop i.e. moisture removal. The experiment is conducted from 10.00 AM to 06.00 PM for a few couples of days. To achieve a steady-state condition the trial of experimental measurement started one hour before the actual measurements were taken. At the end of the day, the color appearance and the weight drop were recorded daily. During the trial of the experiment temperature and humidity at ambient conditions, temperature and humidity at the absorber plate, temperature, and humidity at collector air discharge, and temperature and humidity at the dryer chamber are measured and recorded by the smart Arduino system and further saved into an SD Card. Temperatures and humidity were measured using DHT22 & DHT11 digital sensors which were further connected to the data logging system and LCD screen for continuous monitoring of data points. The velocity of the flow of air is regulated by the fan controller and measured by the anemometer. Also, the pyrometer is used to measure solar radiation.

IV. RESULTS AND DISCUSSION

Thermal Performance of the Device

Graph No.1 represents the variation of time concerning temperature present in the atmosphere, the temperature inside the collector body, the temperature at the absorber surface, and the temperature inside the drying chamber on the first

day of drying. (29th March 2020) which is typically a sunny day. Exactly at 10.00 AM, the drying of grapes started. After 30 minutes, the temperature rise in the drying chamber is observed. The temperature inside the drying chamber is noted maximum from 03.00 PM to 03.30 PM as 41°C.
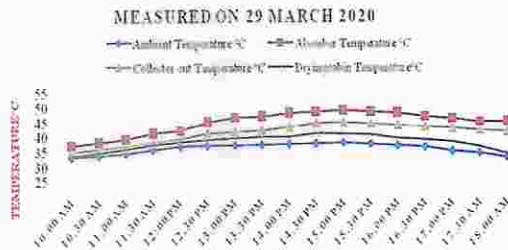
Graph No.1 variations of temperature present in the atmosphere, temperature inside the collector body, temperature at the absorber surface, and temperature inside the drying chamber.
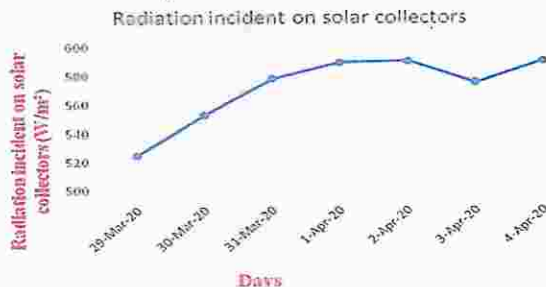

Graph No.2 shows the variation of solar radiation incident on the flat plate collector on 29th march 2020, it is noted that the peak radiation amount is 673 W/m² from 12.30 PM to 01.00 PM.
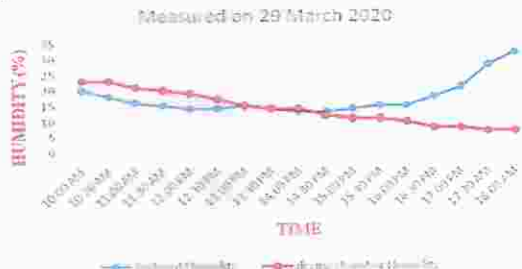
Graph No.3 variations of relative humidity (%) present in the atmosphere and present inside the drying chamber concerning time.

As shown in Graph No. 3 the relative humidity at the beginning of the drying test was almost the same. The incident solar radiations during the start were 660W/m² and the recorded atmospheric temperature was 33.3°C. After a time of 2 hours, solar radiation is raised with 13W/m² which results in a reduction of humidity inside the drying chamber by 4%. After 04.00 PM the humidity in the atmosphere raised by 18% in just two hours, but it does not raise the humidity and moisture content inside the drying chamber. Due to heat trapped by the collector body and absorber surface, the dehumidification continued and reached up to 7% relative humidity.

Graph No.4 variation of solar radiation incident on flat plate collector daily at 02.00 PM

Graph No 4 shows radiation incidents on solar collectors. As per the Nashik altitude collector set as the angle of 19°.

1423

Which gets maximum solar radiation in collectors. In experimental processes, solar radiation gets increases on a sunny day.
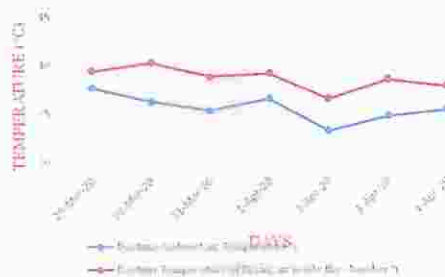
Graph No.5 temperature in the atmosphere and temperature inside the drying chamber of the solar dryer daily at 02.00 PM

Graph No. 5 shows the variation in temperatures in ambient temperature and inside the drying chamber during the period of grapes drying in the solar dryer. As shown in the graph, on 29th March, 1st April and 4th April, due to cloudy weather the temperature gradient between the drying cabin and atmospheric temperature was low as 1.8°C, 2.6°C, 2.4°C but during the sunny days like 30th March and 3rd April the temperature difference between the drying cabin and atmospheric temperature was 3.8°C to 4.2°C.
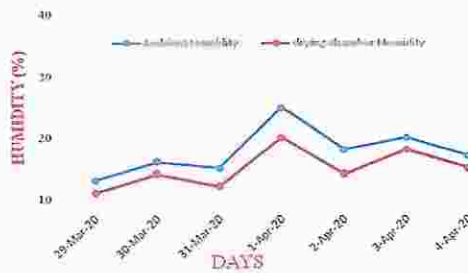
Graph No.6 Relative Humidity in the atmosphere and Relative Humidity inside the drying chamber of solar dryer daily at 02.00 PM.

Graph No. 6 shows relative humidity in the atmosphere and inside the drying chamber. Reading takes at 02.00 PM every day. On 1st April 2020, humidity is high. Humidity, as compared to the atmosphere, is less in the drying chamber which increases the moisture removal rate.

B. Drying behavior of the device
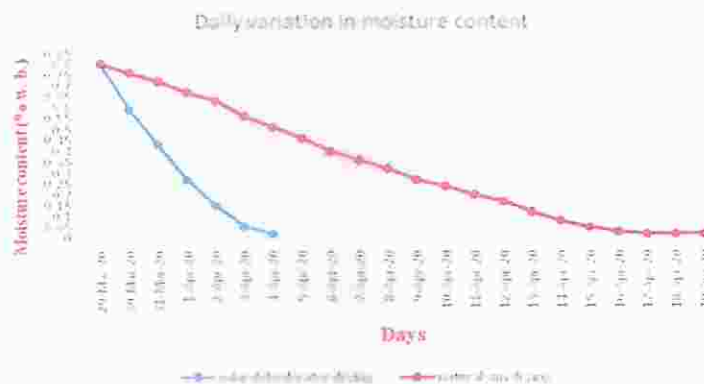
Graph No. 7 Daily variation in moisture content using the solar dryer and without using the solar dryer (Conventional method)

Graph No. 7 shows the daily variation of moisture content of two groups of grapes in which one is kept inside the solar dryer and the other is dried conventionally. Compared to natural drying solar drying required 7 days for complete drying. In natural drying quantity and quality is low due to uneven drying processes.
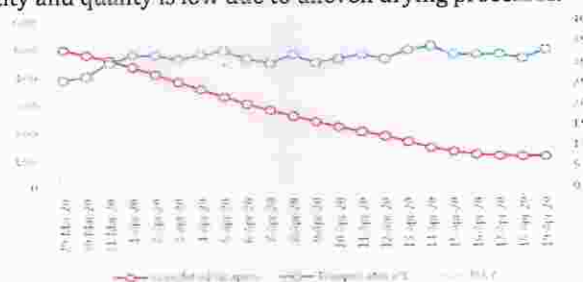
Graph No.8 variation of temperature and weight of raisins concerning days (Conventional drying)

Graph No. 8 shows that the conventional method of drying grapes takes 21 days to convert into raisins. The initial moisture content of grapes was 81%. As the moisture content of grapes reduces, the weight is also reduced. The sample weight of the grape bunch was 500 grams which were reduced to 110 grams. At this stage, it is converted into perfect raisins since the weight drop was stopped after 110 grams.

Fig.5 shows the weight drop from 500 grams to 110 grams and the physical and aesthetical changes of grapes.

Nomenclature:

Ac : Area of the collector (m2)

Hi : Latent heat of vaporization of water (kl/kg)

IR: Solar radiation (w/m^2)

Mw: Mass of water removed (kg)

M: Moisture content of the sample at any time (kg/kg)

C: Specific heat of air at constant volume (J/kg°Q

T: Time (hour)

To: Outlet temperature of air (°Q

Ti: Inlet temperature of air (°Q

mo: Initial total mass (kg)

mi: Initial moisture content sample(kg)

mf: Final moisture content in the sample(kg)

ΔW: difference in weight loss in 1 hour (kg)

ΔT: difference in time (hour)

ɳdryer: Efficiency of the dryer

ɳc: Thermal efficiency of solar collector

A. Solar Dryer Efficiency:

The Thermal efficiency of a solar dryer system ɳdryer is the ratio of the heat required to extract the moisture from food products to the energy required to run the solar dryer

$$\eta d = Mwhi \ / \ Aclt \qquad (1)$$

Here, the prior measured mass of the grape sample was 500 grams, converted into a final mass of 110 grams, resulting in 0.390 kg of water being removed from a sample of 0.5 kg. For measuring the unit mass of 1 kg from the sample 0.78 kg of water is removed. The 9.14% thermal efficiency was found in the drying chamber cabinet.

B. Moisture Removal Rate:

$$Mw = (Wi-Wf)/Wi *100 \qquad (2)$$

We measure the sample's moisture removal rate by taking the sample's initial weight of 500 grams, which was converted into 110 grams. From the above formula, we get the moisture removal rate is 78%.

C. Mass of Water Evaporate from the sample:

$$W = mo(mi-mf)/100-mf \qquad (3)$$

For measurement mass of water evaporate total mass taken is 1 kg which initial moisture content of about 80% after drying we get moisture on the sample is 22% is reaming, therefore the mass of water evaporating from the sample is around 70%.

1426

D. Drying Rate:

$$DR = \Delta W/ \Delta T \qquad (4)$$

The weight of the sample we get is 1 kg after a 1-day drying process weight loss is up to 226 grams. The drying process conducts 6 hours a day which means in 1-hour weight loss of 37.66 grams. Therefore, the drying rate of 37.66 grams/hour.

V.CONCLUSION

A flat-plated indirect-type flat-plate collector solar dehydrator was developed to investigate the performance of drying grapes. The following conclusions have been drawn from the results: The temperature inside the drying chamber cabinet remains higher than the ambient temperature. The result of grapes drying is shown that the mass of 500-gram grapes converted into 110 grams of perfect raisins. The maximum output temperature of 59°C can be achieved. The average thermal efficiency of the solar dryer using a flat plate collector is 9.14%.

BIBLIOGRAPHY

[1]Ashish D. Chaudhari, Prof. Sanjay P. Salve, "A review of solar dryer technologies", international journal of research in advent technology, vol.2, No.2, February 2014.

[2]Jarinee Jongpluempiti, Nattadon Pannucharoenwong,"Design and construction of the flat plate solar air heater for spray dryer", International conference on Alternative energy in developing countries and emerging economies, May 2017.

[3] Syed MohammedShamiq, P Sudhakar, M cheralathan," Experimental Study of a solar dryer with different flow patterns of air in the drying chamber", ICAME 2018.

[4]Adit Rana, Ranchan Chauhan, MuneeshSethi,"Experimental Investigation of the performance of tubular solar dryer", International advanced research journal in science, Engineering and technology CETCME-2017.

[5]Majedul Islam, MdImrulLslam, MehediTusar,"Effect of cover design on moisture removal rate of a cabinet type solar dryer for food drying application", International conference on energy and power, ICEP2018,13-15 December 2018.

[6]Hajar Essalhi, RachidTadili, M.N Bargach,"Conception of a solar air collector for an Indirect solar dryer. Pear drying Test.", International conference on power and energy systems Engineering, September 2017.

[7]UmeshToshiwal, S.R Karale," A review paper on solar dyer", International journal of engineering research and applications, vol.3, Issue2, March- April 2013.

[8]Isaac NyambeSimate, Sam Cherotich,"Design and testing of a natural convection solar tunnel dryer for mango", Hindawi Journal of solar energy, volume 2017, Article ID 4525141.

[9]Jyoti Singh, "Review paper of study on solar dryer", Journal of Mechanical and Mechanics Engineering, Vol.1, Issue 1.

[10]ShrideviMadhavan, Dr. P N Ramachandran," Design, Fabrication, and testing of a solar paper dryer", International research journal of engineering and technology, Vol.2, Issue 4, July 2015.

[11]Anna Hubackova, Iva Kucerova,"Development of Solar Drying Model for Selected Cambodian Fish Species" Hindawi Publishing Corporation, The Scientific World Journal Volume 2014, Article ID 439431

IQAC In-charge
Rajiv Gandhi College of Engineering
Karjule Harya, Tal. Parner
Dist. Ahmednagar-414304

Principal
R G COE, Karjule Harya.

Implementation of Google Studio and Taguchi DOE to minimize the Resultant Vibration in Hard Turning

Dr. Krupal Prabhakar Pawar[1*]
Associate Professor, Mechanical Engg. Department, Rajiv Gandhi College of Engineering, Karjule Harya[1]
Email: krupalpawar@gmail.com

Abstract

The present investigation is related to the implementation of Google Studio and Taguchi DOE for parametric optimization of the turning process of hard AISI M2 grade material. The main aim of the present investigation was to minimize the resultant vibration during the turning process of AISI M2 on the CNC Machine. In this study, the whole experimentation has done in dry conditions. The process parameters selected for the investigation was Cutting Speed, Feed Rate, Depth of Cut, and resultant vibration selected as quality response characteristic. The material AISI M2 hardness during experimentation was 62-64 HRC. This hardness is selected for the study because this is the actual hardness of the drill tool. Google Studio is employed to generate results and data analysis. The MINITAB 21.2 software is used to design the experiment. The turning process optimization is done using Taguchi Method and Google studio. It is concluded that the feed rate is the most significant machining parameter which affects the resultant vibration signal. The optimum level of process parameters is cutting speed= 180 mm/min, feed rate= 0.1 mm/rev, and depth of cut = 0.4 mm.

1. INTRODUCTION

In today's world, a great deal of attention is placed on investigating vibration signals in various machining operations, such as drilling, milling, turning, and so on. Studying and optimizing the resultant tool vibration signals in the machining process is very important. This is because minimizing the resultant vibration signal allows us to obtain various benefits, such as the minimum possible tool wear, a better surface finish, increased tool life, and increased productivity due to the minimum setting time for the machine. Because of these benefits, it is very important to minimize the resultant vibration signal.

Abouelatta, O. B. et al. [1], "employed an FFT analyzer to measure tool vibration in the radial direction and feed direction and for measurement of surface roughness the Surtronic 3+ measuring instrument used and correlation between surface roughness and cutting vibration during turning established. They developed a mathematical model for the predicted roughness parameter based on the cutting parameter and machine tool vibration for a better understanding of the relation. Finally, the measured results were analyzed by commercial software MATLAB, BC++, and SPSS."

Bhuiyan. M. S. H. et al. [2], "investigated various sensors used to monitor tool conditions using optical, electrical, and magnetic signals. They studied transient elastic waves generated during machining known as acoustic emission (AE). They proposed the use of an acoustic emission sensor and tri-axial accelerometer placed on a shank of the cutting tool holder was capable to monitor tool condition. The acoustic emission sensor assessed the internal change whereas the vibration sensor asses' the external information of the tool state. They illustrated the use of RMS signal and fast Fourier transform as the output of the sensor. They proved that vibration components, Vx, Vy, and Vz change with feed rate, depth of cut, and cutting speed respectively. The amplitude of vibration components decreases with the increase of cutting speed and increases with the increase of feed rate and depth of cut."

Alonso, F. J., and Salgado, D. R. [3], "developed a reliable tool condition monitoring system (TCMS) for industrial application. They employed singular spectrum analysis (SSA) and cluster analysis for analysis of the tool vibration signals. SSA was a non-parametric technique, of time series analysis that decomposes the acquired tool vibration signals, and Cluster analysis was used to group the SSA decomposition in order to obtain several independent components in the frequency domain that are applied to feed-forward back-propagation (FFBP) neural network to determine the tool flank wear."

IQAC In-charge
Rajiv Gandhi College of Engineering
Karjule Harya, Tal. Parner
Dist. Ahmednagar-414304

Principal
R G COE, Karjule Harya.

Aliustaoglu, C. et al. [4], "studied tool wear condition monitoring using a sensor fusion model based on a fuzzy inference system. They mainly concentrated on the drilling and milling operation. They used two-stage fuzzy logic schemes for developing the advanced tool condition monitoring system. They acquired signals from various sensors and processed them to decide the status of the tool. In the first stage, they derived statistical parameters from thrust force, machine sound (acquired via a very sensitive microphone), and vibration signals were used as inputs to the fuzzy process; the crisp output values of this process were then taken as the input parameters of the second stage. Conclusively, outputs of this stage were taken into a threshold function, the output of which was used to assess the condition of the tool."

Bhuiyan, M. S. H. et al. [5], "studied the tool wear, chip formation, and surface roughness of workpieces under different cutting conditions in machining using acoustic emission (AE) and vibration signature in turning. The investigation concluded that the acoustic emission and vibration components can effectively respond to different occurrences in turning including tool wear and surface roughness. The acoustic emission has shown a very significant response to tool wear progression whereas resultant vibration (V) represented surface roughness in turning. Vibration components Vx, Vy, and Vz described the chip formation type and increase with the increase of feed rate, depth of cut, and cutting speed respectively. A KISTLER 8152B AE-piezoelectric sensor with a sensitivity of 57 dB ref 1 V/(m/s) and a KISTLER 8762A50 tri-axial accelerometer with a sensitivity of 100 ± 5% mV/g were used. They captured raw acoustic emission and vibration sensors analyzed to determine the different occurrences, including the tool wear and surface roughness of the workpiece. The data from direct measurement of flank wear and surface roughness, and chip formation occurrences were utilized to justify the signals response, and thus to investigate the tool condition even more accurately. The output signals from the acoustic emission and vibration sensors were essentially complex and stochastic in nature. The acoustic emission and vibration signature performed exceptionally well to investigate the tool state and the different turning occurrences. The combined application of acoustic emission and vibration sensors described the tool wear, tool breakage, chip formation, chip breakage, machine tool vibration, machine vibration, and workpiece surface roughness."
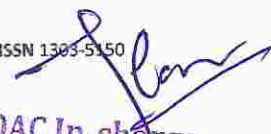
Kilundu, B. et al. [6], "presented the singular spectrum analysis (SSA) for the analysis of vibration signal from the tool holder. They explored the use of data mining techniques for tool condition monitoring in metal cutting. They also performed Pseudo-local singular spectrum analysis (SSA) on vibration signals measured on the tool holder. Then this is coupled to a band-pass filter to allow the definition and extraction of features that are sensitive to tool wear. These features are defined in some frequency bands, from sums of Fourier coefficients of reconstructed and residual signals obtained by SSA. They also studied two important aspects the strong relevance of information in high-frequency vibration components and the benefits of the combination of SSA and band-pass filtering to get rid of useless components (noise)."

Abuthakeer, S. S. et al. [7], "used a damping pad made from neoprene to control the cutting tool vibration. The experiment was carried out in fewer than two cases with the use of a damping pad and without a damping pad on the CNC LATHE machine. They developed an empirical model using analysis of variance (ANOVA). They also used a multilayer perception neural network model constructed feed-forward back-propagation algorithm using the acquired data. On the completion of the experimental test, ANN was used to validate the results obtained and also to predict the behavior of the system under any cutting condition within the operating range."

Krupal Pawar et al. [12] "investigated the effect of insert nose radius and machining parameters including cutting speed, feed rate, and depth of cut on surface roughness (Ra) and material removal rate (MRR) in a turning of HSS (M2) using the Taguchi method and ANOVA. A three-level, four-parameters design of experiment, L9 orthogonal array using Minitab 14 software, the signal-to-noise (S/N) ratio is employed to study the performance characteristics in the turning of HSS (M2) by taking the nose radius of Tin coated carbide inserts tool of 0.4, 0.8 and 1.2 mm on CNC turning centre. The analysis of variance (ANOVA) is applied to study the percentage contribution of each machining parameter while CNC turning of HSS (M2) material. All experimental trials are conducted in dry machining environment and at a constant spindle speed of 2800 rpm. The results are verified by taking confirmation experiments. The present investigation indicates that feed rate and nose radius are the most significant factors in the case of material removal rate and surface roughness for turning HSS (M2) material."

By studying various papers, it is concluded that no work is found for optimizing the resultant vibration for hard (62-64 HRC) AISI M2 using Google studio and Taguchi DOE with help of MINITAB 21.2. This

investigation demonstrates details of the Taguchi optimization technique to optimize the resultant vibration signal during hard turning. The main objective of the present study is to find out set machining parameters which result in minimum resultant vibration signal in Hertz while turning hard AISI M2 on a CNC machine.

2. EXPERIMENTATION SETUP AND CUTTING CONDITIONS

For the conducting experimental trials, the ACE make CNC model Simple Turn-5075 Siemens 802C is employed (see Fig.2). First of all, it is very important to select a process with process parameters and their levels. In the research work, machining parameters such as cutting speed, feed rate, and depth of cut are selected for optimization of resultant vibration. The three parameters with three levels are fixed with the help of the insert manual and machining handbook (see Table.1). In the present research work, we are going to utilize the Taguchi method for experiment design. The design of the experiment is done with help of MINITAB 21.2 software and for this condition suited orthogonal array such as L27 is selected from the series of arrays. The design of experimental trials is shown in Table 2.

Table 1. Control Factors with Levels

Levels	Control Parameters		
	Cutting Speed (mm/min)	Feed Rate (mm/rev)	Depth of Cut (mm)
L1	100	0.1	0.4
L2	140	0.15	0.5
L3	180	0.2	0.6

The AISI M2 material rods with 60 mm diameter and 350 mm length are selected for experimental trials. The chemical analysis of AISI M2 material C-0.86/0.96, Cr-3.8/4.5, Mo-4.9/5.5, W-6.0/6.75, V-1.7/2.2[10] and the properties of AISI M2 are density-8.028×10-3g/mm3, melting point-46800, hardness-62-65 HRC, compressive yield strength-3250 Mpa, Poisson's ratio-0.27-0.30, elastic modulus-190-210 Gpa [10]. In the present work, a rectangular shape PCBN CNMG 160408 insert (Kennametal company) is used as a cutting tool used for turning hard AISI M2 specimens. The clearance angle of the selected insert is zero. The inscribed circle size is 9.5mm and the thickness is 5mm. A tool holder such as PCLNR 2525M12 is employed to hold the insert.

After DOE, it is important to conduct all trials as per the design of the experiment. The RT-Pro photon software is first installed in the laptop to support the FFT analyzer. The vibration signal frequency in three directions (Vx, Vy, and Vz) are measured using an FFT analyzer with a three-axis accelerometer and after measuring signals, the resultant vibration signals are calculated and inserted in the already design of experiment table in MINITAB 21.2 software. After inserting resultant vibration signals in the MINITAB 21.2 software, the signal-to-noise ratios for each trial is calculated by applying the smaller is better condition.

$$S/N = -10 \times log(\Sigma(Y^2)/n)) \tag{1}$$

Where, S/N-Signal to Noise Ratio, Yi – i[th] observed value of the response, n - Number of observations in a trial, Y - Average of observed responses values.

Figure 2. Experimental Unit

Table 2. Experiment Conduction as DOE

Exp. No.	Cutting Speed	Feed Rate	Depth of Cut	Vr (Hz)	S/N Ratio (dB)
1	100	0.1	0.4	2744.52	-69.08
2	100	0.1	0.5	3343.94	-70.74
3	100	0.1	0.6	2666.56	-68.84
4	100	0.15	0.4	3325.41	-70.69
5	100	0.15	0.5	3301.44	-70.63
6	100	0.15	0.6	3349.09	-70.75
7	100	0.2	0.4	3308.10	-70.65
8	100	0.2	0.5	3305.21	-70.64
9	100	0.2	0.6	3239.84	-70.47
10	140	0.1	0.4	3335.84	-70.72
11	140	0.1	0.5	3266.57	-70.54
12	140	0.1	0.6	3264.80	-70.54
13	140	0.15	0.4	3329.06	-70.70
14	140	0.15	0.5	3327.28	-70.70
15	140	0.15	0.6	3323.36	-70.69
16	140	0.2	0.4	2766.92	-69.15
17	140	0.2	0.5	3326.14	-70.70
18	140	0.2	0.6	3333.62	-70.72
19	180	0.1	0.4	2547.98	-68.46
20	180	0.1	0.5	3162.74	-70.27
21	180	0.1	0.6	2710.94	-68.98
22	180	0.15	0.4	3439.86	-70.73
23	180	0.15	0.5	2827.03	-69.03
24	180	0.15	0.6	3421.24	-70.68
25	180	0.2	0.4	3450.82	-70.76
26	180	0.2	0.5	3389.91	-70.60
27	180	0.2	0.6	3386.19	-70.59

The calculation of signal-to-noise ratios with help of MINITAB 21.2 software is shown in the following Table 2.

3. RESULTS AND DISCUSSION

Figure 3. indicates the evolution of the resultant vibration signal according to the three machining parameters. Figure 3. shows that the resultant vibration signal is minimum at a cutting speed of 180 mm/min. It shows that at a cutting speed of 180 mm/min, the resultant vibration signal is at an optimum level means we will get a smooth operation with minimum resultant vibration at 180 mm/min. The feed rate is the most influencing factor for the resultant vibration signal. The resultant vibration at 0.1 mm/rev is at the minimum stage.
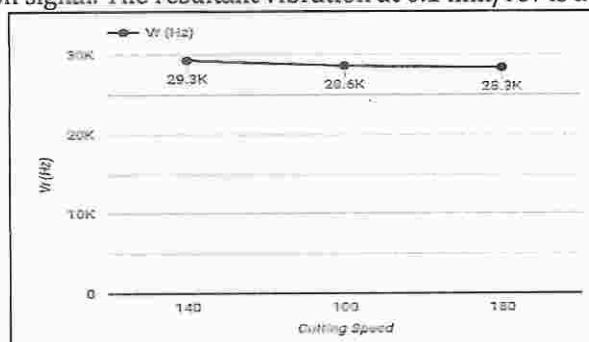
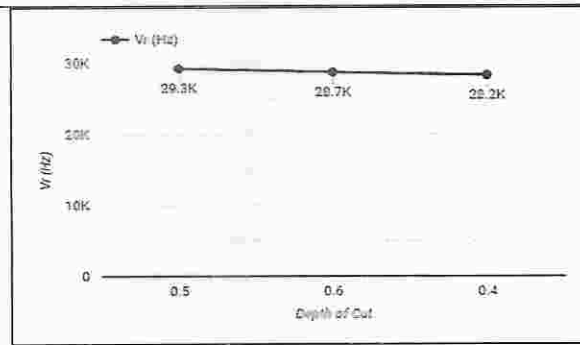(a) Resultant Vibration (Vr) vs Cutting Speed

(b) Resultant Vibration (Vr) vs Depth of Cut
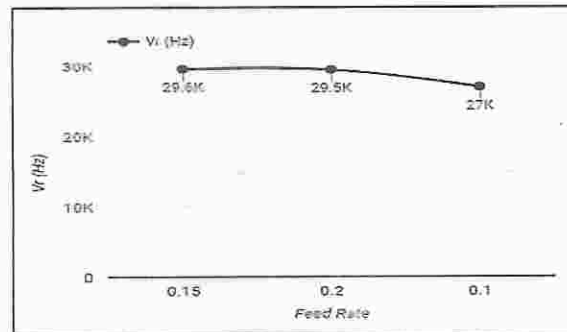
(c) Resultant Vibration (Vr) vs Feed Rate

Figure 3. Plots using Google Studio for Resultant Vibration Vs. Machining Parameters
(i.e. Cutting Speed, Depth of Cut, and Feed Rate)

6. CONCLUSION

It is concluded that for turning the hard AISI M2 tool steel, the feed rate is the more important machining parameter that affects the resultant vibration signal. The optimum level of process parameters is cutting speed= 180 mm/min, feed rate= 0.1 mm/rev, and depth of cut = 0.4 mm at which we get the minimum resultant vibration. In this research, we have implemented Google Studio for data visualization. Google Studio is the best tool for data visualization, filtering, and clearing data.

BIBLIOGRAPHY

[1] Abouelatta, O. B., & Madl, J. (2001). Surface roughness prediction based on cutting parameters and tool vibrations in turning operations. Journal of materials processing technology, 118(1-3), 269-277.

[2] Bhuiyan, M. S. H., Choudhury, I. A., & Nukman, Y. (2012, July). Tool condition monitoring using acoustic emission and vibration signature in turning. In Proceedings of the world congress on engineering (Vol. 3, pp. 1-5).

[3] Alonso, F. J., & Salgado, D. R. (2008). Analysis of the structure of vibration signals for tool wear detection. Mechanical systems and signal processing, 22(3), 735-748.

[4] Aliustaoglu, C., Ertunc, H. M., & Ocak, H. (2009). Tool wear condition monitoring using a sensor fusion model based on fuzzy inference system. Mechanical Systems and Signal Processing, 23(2), 539-546.

[5] Bhuiyan, M. S. H., Choudhury, I. A., & Dahari, M. (2014). Monitoring the tool wear, surface roughness and chip formation occurrences using multiple sensors in turning. Journal of Manufacturing Systems, 33(4), 476-487.

[6] Kilundu, B., Dehombreux, P., & Chiementin, X. (2011). Tool wear monitoring by machine learning techniques and singular spectrum analysis. Mechanical Systems and Signal Processing, 25(1), 400-415.

[7] Abuthakeer, S. S., Mohanram, P. V., & Kumar, G. M. (2011). Prediction and control of cutting Tool vibration in CNC Lathe with ANOVA and ANN. International Journal of Lean Thinking, 2(1), 1-23.

[8] FFT Analyzer User Manual.

IQAC In-charge
Rajiv Gandhi College of Engineering
Karjule Harya, Tal. Parner
Dist. Ahmednagar-414304

Principal
R G COE, Karjule Harya.

[9] AEC make CNC model simple turn 5075 user manual.

[10] HSS (M2) data sheet, Bohler-Uddeholm.

[11] Krishnaiah, K., & Shahabudeen, P. (2012). Applied design of experiments and Taguchi methods. PHI Learning Pvt. Ltd..

[12] Pawar, K., & Palhade, R. D. (2015). Multi-objective optimization of CNC turning process parameters for high speed steel (M2) using Taguchi and ANOVA method. International Journal of Hybrid Information Technology, 8(4), 67-80.

1410

Investigation of Performance Analysis for Composite Helical Compression Spring and Steel Compression Spring

Dr. Krupal Pawar[1*], D.S. Dhondage[2]

Associate Professor, Mechanical Engg. Department, Rajiv Gandhi College of Engineering, Karjule Harya[1]
Assistant Professor, Mechanical Engg. Department, Sandip University, Nashik[2]
Email:krupalpawar@gmail.com

Abstract

The current work is focused on studying and analyzing spring design with the goal of replacing traditional steel material with composite material such as Kevlar, epoxy glass, and epoxy carbon. Experiments will be carried out to verify the conventional spring's static deflection and stiffness. These experiments will make use of the finite element approach, which is implemented inside ANSYS software. By using the finite element approach in ANSYS, we will determine the static deflections and stiffness of every composite spring. The stiffness of composite springs and traditional springs will be evaluated, and a recommendation will be made for the best material overall. The design of the spring will be evaluated with regard to the weight of the bike, as well as the weight of a single person and of two people riding together. CATIA V5 and ANSYS are the programs that are used to do the modeling and analysis, respectively. Existing springs and those made of brand-new material will both be used as points of comparison in this research. In FEA, static analysis is the process that determines the stresses and deflections caused by helical compression.

Key Words: *Composite Material, ANSYS, FEA, Helical Coil Steel Spring, CATIA V5.*

1411

I. INTRODUCTION

The primary purpose of the helical compression spring is to act as a shock absorber, dampen vibrations, and make the driving experience more comfortable for the operator. In the manufacturing business, springs are used primarily as members for the purpose of absorbing shock energy and restoring the original position of a component after it has been displaced for the purpose of commencing a particular function. Compression springs are helical coil springs that are designed to withstand an axially applied compressive force. Compression springs may have a variety of different shapes, including cylindrical, conical, tapered, concave, or convex. The research that is being done in the automotive industry right now is mostly focused on the utilization of unconventional materials in lieu of traditional materials. Composite materials are an alternative to traditional materials that are employed in many of the components of cars. A composite material is one that is made up of a blend of two or more different types of materials. When compared to traditional materials, components made using composite materials have a lower overall weight while retaining the same level of mechanical strength as those made with traditional materials. This results in the solution to the challenge of weight reduction that the automotive manufacturing industry will confront in a few decades. Typically made from round wire, coil compression springs are twisted in the shape of a helix. Cyclic loading is applied to the spring on a regular basis for the purpose of the application in question, and the greatest frequency of use that is anticipated is between 5 and 50 cycles per minute. When considering the anticipated service life of 10–15 years, the spring should be able to endure cyclic compression loads for a few million times at the very least. The springs need to have a design that ensures their dependability. The springs need to be constructed such that they can sustain the cyclic loading that occurs when the machine is in operation. As a result, it has been suggested that the design and fatigue study of a compression spring be carried out as part of this research effort in order to achieve superior performance in terms of long service life.

II. LITERATURE SURVEY

For the study point of view, we have selected some research articles which are mentioned as follows:

I Balaguru, et al. (2016) [1] "suggested the improvement of fuel efficiency of vehicles by reducing the weight of the vehicle. They examined design and production methods for FRP composite helical springs and drew the following conclusions: Carbon fiber springs are lighter than glass and glass/carbon fiber springs. Carbon fiber coil springs are stiffer than conventional varieties. Glass fiber/carbon fiber springs perform poorly compared to other varieties. Braided + Unidirectional + Rubber core offers greater mechanical qualities than Unidirectional, Unidirectional+ Rubber core, and Outer braid + Unidirectional. Composite helical springs may be substituted in lightweight automobiles with a little size compromise. In ordinary automobiles, combining composite and conventional springs may overcome the poor rigidity of composites and optimize spring weight".

1412

D. Abdul Budan et al. (2010) [2] "investigated the feasibility of composite coil springs for Automotive Applications. They showed that composite coil springs can replace metal ones. Glass fiber, carbon fiber, and a mixture were used to make springs. The study aims to minimize spring weight. The carbon fiber spring rate is 34% higher than the glass fiber spring and 45% higher than the glass fiber/carbon fiber spring. Carbon fiber springs are 18% lighter than glass fiber, 15% lighter than glass fiber/carbon fiber, and 80% lighter than steel. Composite springs are lighter and stiffer than steel springs. (A steel spring of the same size springs 14 N/mm and weighs 1.078 kg.) These springs' experimental findings led to the following conclusions. Carbon fiber springs are lighter than glass and glass/carbon fiber springs. Carbon fiber coil springs are stiffer than conventional varieties. Glass fiber/carbon fiber roving springs perform poorly compared to other varieties".

Bok-Lok Choi a., et al. (2015) [3] "investigated numerical and experimental methods for determining the ply angles and wire diameters of carbon fiber/epoxy composite coil springs to attain a spring rate equal to that of an equivalent steel component. The inverse connection between twist angle and shear modulus predicted the composite's equivalent shear modulus. The shear modulus for a composite with a 450 ply angle was 16.8% of that of steel, and the calculated shear modulus was in excellent accord with experimental data. With an optimal ply angle of 450, a composite coil spring's wire diameter will be 17.17 mm. FEA and experimental findings for a composite coil spring with a 450 ply angle agreed well. Applying the proposed analytical and experimental approaches to a composite coil spring resulted in a 55% weight reduction".

M. Sudheer, et.al. (2015) [8] "studied the Analytical and Numerical Validation of Epoxy/Glass Structural Composites for Elastic Models. Elastic characteristics like Young's modulus (E1 and E2) and Poisson's ratio (v12 and v21) are assessed for n various volume fractions along the material's primary directions (FEM). The solver was ANSYS. These computer conclusions are contrasted with analytical results from the Rule of a mixture, Halpin-Tsai, Nielsen, and Chamis elastic models. This work compared computational and analytical data to find the optimal elastic characteristics. The Epoxy/Glass composite is more effective when loaded along the fiber direction".

Sujit S Patil, et. al. (2016) [9] "analyzed that the composite helical springs can be effectively used in automobiles without affecting the performance of the suspension system of the vehicles. They're 50%-70% lighter than steel springs. E-glass/Epoxy spring costs 20% more than steel but is 50% lighter with the same performance. Carbon/Epoxy springs are 5 times more expensive than steel but much lighter. Composite spring stiffness is similar to steel. Suspension systems can successfully employ composite springs".

Sid Ali Kaouaa, et. al. (2011) [4] "presented a 3D geometric modeling of a twin helical spring and its finite element analysis to study the spring mechanical behavior under tensile axial loading. Using computer-aided design (CAD) tools, a finite element model is produced to create the graphic design of the spiraling form. As a result, the complicated "wired shape" of the spring is discretized using 3D 18-DOF pentameric components, enabling the measurement of the mechanical reaction of the twin spiraled helical spring under an axial load. With sinusoidal behavior, the analysis shows a strong correspondence between the evolution of the theoretical and numerical tensile and compression normal stresses. The internal radial zone at section 1800 has the highest value of the total equivalent stress ISO values, which grow radially from 00 to 1800. On the other side, the filament cross-center section's is where the least amount of tension is present".

Wang, F. (2001) [10] "discussed the active suspension control of vehicle models. It contains two main parts. First, mechanical network analysis showed the need for active suspension. He used conventional network

www.neuroquantology.com

theory to prove that half- and full-car models need active suspension in certain conditions. When a soft passive suspension is used for road disturbances, a firm passive suspension is used for load disturbances. In the second phase of the study, he parametrized all stabilizing controllers for a specific plant while fixing a closed-loop transfer function. He defined left and right normal rank factorizations of a rational matrix to aid parametrization. Under some situations, the residual transmission pathways' performance may approach the original set. The findings are then used to create controller architectures for quarter-, half-, and full-car models. He outlined the basic assumptions needed to decompose a half-car into two quarter-cars. He uses symmetry to partition a full-car model into bounce/pitch and roll/warp half-car models. Warp mode reduces chassis twisting forces. For complicated models, numerical controller structure calculations are described and applied to double-wishbone models. The trailing-arm model illustrates his work's primary concepts. He explains anti-squat and anti-dive trailing-arm design. Network analysis suggests an active suspension to meet performance objectives. This model's active suspension is designed using disturbance response decoupling. AutoSim was utilized to simulate car models together with theoretical studies during this endeavor. This research's analysis and synthesis approaches may be used to complicated models".

1413

Skewis, W. H. (2017) [7] "experimentally examined Very high cycle fatigue (VHCF) properties of a newly developed clean spring steel under rotating bending and axial loading. This steel has the duplex S–N property solely for surface-induced failure under rotational bending, but only the single S–N property under axial stress. This steel's VHCF failure mechanism is a minor grinding defect-induced failure. The surface morphology of the interior inhomogeneous microstructure with distinct plastic deformation is much rougher than that of the ambient matrix, which means stress concentration from strain inconsistency between the microstructural inhomogeneity as the soft phase and the ambient matrix as the hard phase causes interior crack initiation. The threshold stress intensity factor for surface small defect-induced fracture propagation of this steel is 2.04 MPam1/2, which suggests the short crack effect plays a crucial role in inducing surface small defect-induced failure in the VHCF regime. Under a certain flaw density, surface and interior failure probability are similar. If the inner defect size is less than or equal to the surface defect size, surface defect-induced failure will dominate in VHCF, particularly under rotational bending".

Michalczyk, K. (2013) [5] "presented the analysis of elastomeric coating's influence on dynamic resonant stressed values in spring. The appropriate equations determining the effectiveness of dynamic stress reduction in resonant conditions as a function of coating parameters were derived. It was proved that rubber coating will not perform in a satisfactory manner due to its low modulus of elasticity in shear. It was also demonstrated that about-resonance areas of increased stresses are wider and wider along with the successive resonances and achieve significant values even at large distances from the resonance frequencies"

Pyttel, B., et.al.(2014) [6] "conducted Long-term fatigue tests on shot-peened helical compression springs by means of a special spring fatigue testing machine at 40 Hz. Test springs were made of three different spring materials – oil-hardened and tempered SiCr- and SiCrV-alloyed valve spring steel and stainless steel. With a special test strategy in a test run, up to 500 springs with a wire diameter of d = 3.0 mm or 900 springs with d = 1.6 mm were tested simultaneously at different stress levels. Based on fatigue investigations of springs with d = 3.0 mm up to a number of cycles N = 109 an analysis was done after the test was continued to N = 1.5 × 109 and their results were compared. The influence of different shot peening conditions was investigated in springs with d = 1.6 mm. Fractured test springs were examined under an optical microscope, scanning electron microscope (SEM), and by means of metallographic microsections in order to analyze the fracture behavior and the failure mechanisms. The paper includes a comparison of the results of the different spring sizes, materials, number of cycles, and shot peening conditions and outlines further investigations in the VHCF region".

The current study demonstrates how composite materials may successfully replace steel springs in helical compression springs used in vehicles. These springs are used in a compression configuration. In this experiment, the performance characteristics of composite helical springs are contrasted with those of a steel spring taken at random from a two-wheeler vehicle.

III. RESEARCH OBJECTIVE

In the past, ordinary steel was used in suspension systems as a helical coil spring to increase performance. Although conventional steel is more affordable and durable than alternative materials, its weight poses a

serious obstacle to its application. The research focuses on the use of composite materials to reduce the weight of springs. Therefore, we chose a composite material that can provide an average performance while using little weight. Additionally, it has improved stiffness, elastic strength, and fatigue characteristics.

IV. METHODOLOGY
The suggested technique is divided into three distinct stages.
Phase 1: Analytical calculations are compared to a traditional finite element study of a steel spring.
Phase 2: Experimental investigation to determine static deflection for steel material using a standard spring.
Phase 3: Composite material Finite Element Analysis (Glass Epoxy, carbon epoxy, and Kevlar).

1414

V. ANALYSIS OF SPRING
Utilizing ANSYS 16.0, a static analysis of the spiral spring design is done to determine the maximum safe stress for the appropriate payload. Hero Passion Motorcycle helical spring is analyzed as a conventional spring utilizing the following three loading scenarios:

Table 1: Loading Conditions for Study

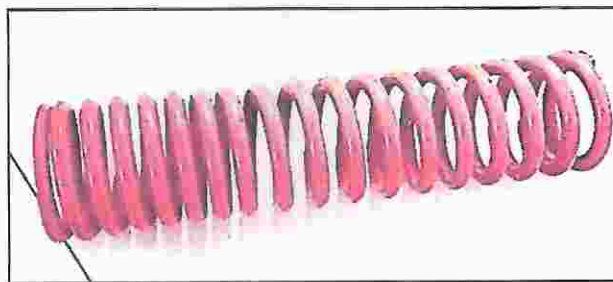| Case No	Load	Loading Conditions
1.	735 N	Wt. of Motorcycle
2.	1176 N	Wt. of bike + 1Person wt
3.	1618 N	Wt. of bike + 2 Person wt.

Figure 1. Hero Passion Motor Cycle Helical Steel Spring

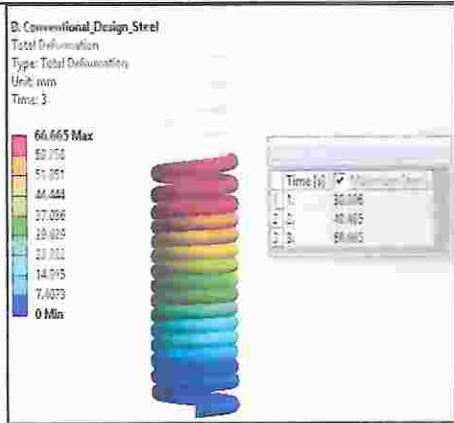Figure 2 Model of conventional steel spring using CATIA V5

IQAC In-charge
Rajiv Gandhi College of Engineering
Karjule Harya, Tal. Parner
Dist. Ahmednagar-414304

Principal
R G COE, Karjule Harya.

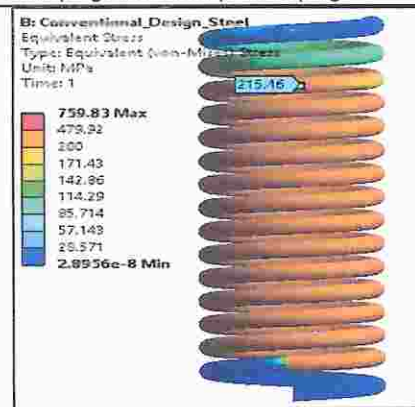**Figure.3** Static Deflection in Steel Spring

Figure.4 Stress Plot Load Case1Related to
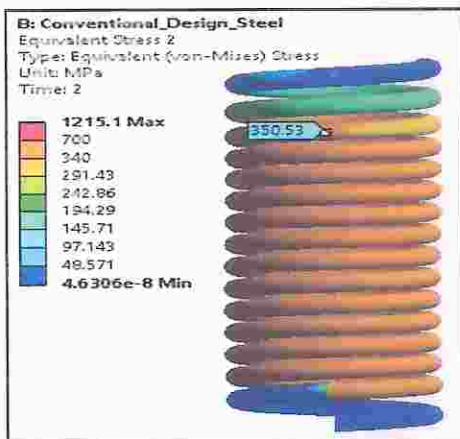Steel Spring

1415

Figure.5 Stress Plot Load Case 2 Related to
Steel Spring

Figure.6 Stress Plot Load Case 3 Related to
Steel Spring

Three load cases are defined to simulate three different cases mentioned in the objective. Figure. 4, Figure.5, and Figure. 6 show the conventional steel spring in three loading conditions.
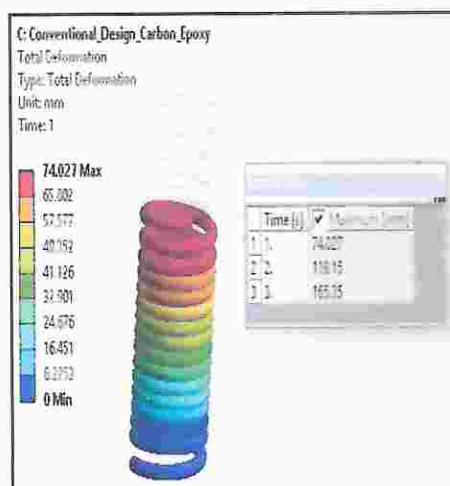
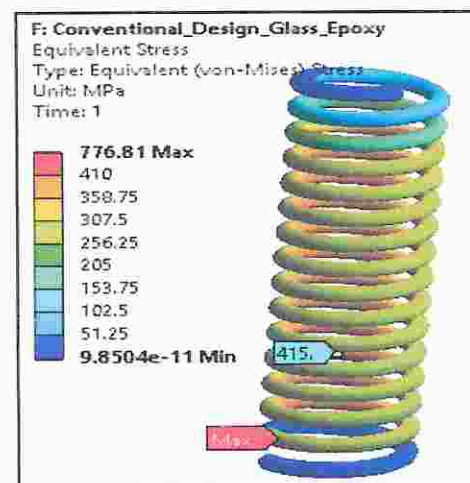

Figure.7 Static Deflection in Glass Epoxy material

Figure.8 Stress Plot Load Case1 Related to
Glass Epoxy material
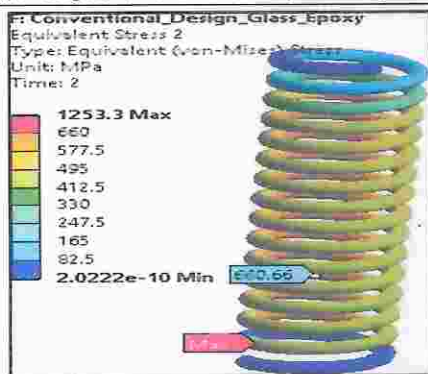
Figure 9. Stress Plot Load Case 2
Related to Glass Epoxy material
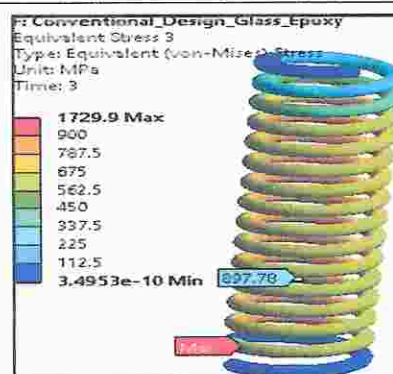
Figure10. Stress Plot Load Case 3
Related to Glass Epoxy material

1416
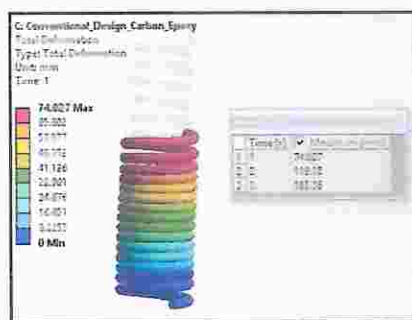
Figure 11. Static Deflection in Carbon Epoxy
Material
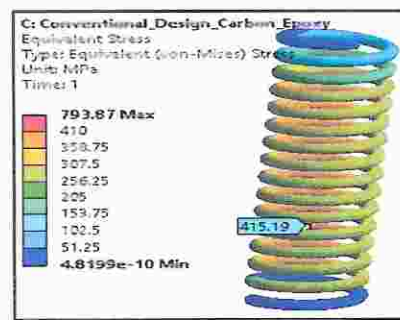
Figure 12. Stress Plot Load Case Related to
Carbon Epoxy Material
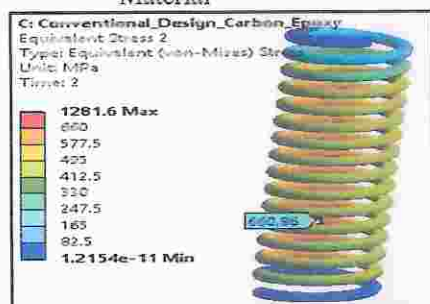
Figure 13. Stress Plot Load Case 2 Related to
Carbon Epoxy Material
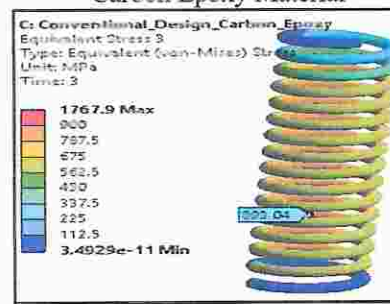
Figure 14. Stress Plot Load Case 3 Related to
Carbon Epoxy Material
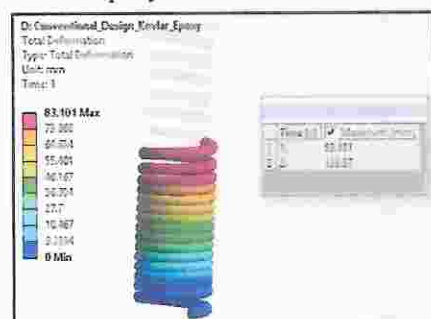
Figure15. Static Deflection in Kevlar Material
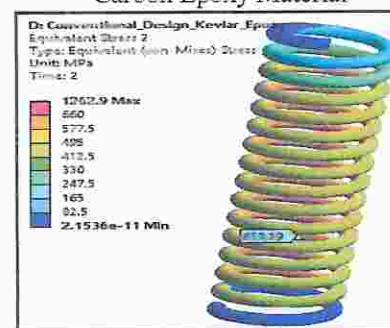
Figure 16. Stress Plot Load Case 1 Related to
Kevlar Material
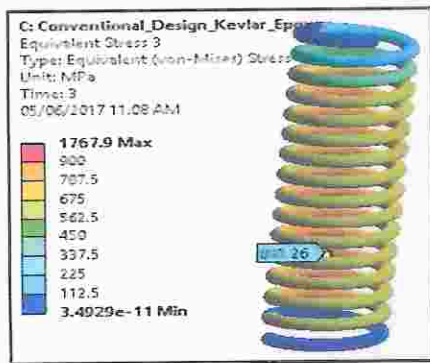
Figure 17. Stress Plot Load Case 2 Related to Kevlar Material   **Figure 18.** Stress Plot Load Case 3 Related to Kevlar Material
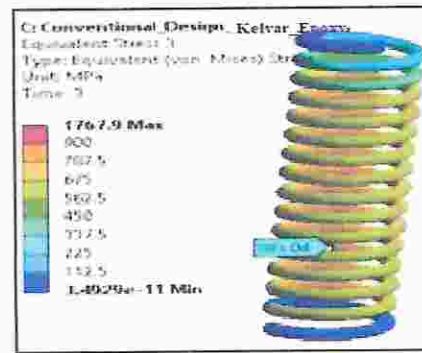
VI. RESULTS AND DISCUSSION

The results of the investigation are summarized as follows:

Table 2. Static Deflection in Steel Spring

Case No.	Load	Weight Combination	Static Deflection (mm)		
			FEA Value	Analytical Value	Experimental Value
1.	735 N	Wt. of bike	29.40	30.00	29.60
2.	1176 N	Wt. of bike + 1 person	47.70	49.00	49.20
3.	1618 N	Wt. of bike + 2 person	68.11	67.00	67.32

Table 3. Bending Stress in Steel Spring

Case No.	Load	Bending Stress (MPa)		
		FEA Value	Analytical Value	% Variation
1.	735 N	214	219	-2%
2.	1176 N	349	351	0%
3.	1618 N	486	483	1%

Table 4. Comparison of Static Deflection in Composits

Case No.	Load	Static Deflection (mm)			
		Steel Material	Glass Epoxy Material	Carbon Epoxy Material	Kevlar Epoxy Material
1.	735 N	31.31	81.385	75.027	84.101
2.	1176 N	49.47	130.49	120.15	134.87
3.	1618 N	67.67	180.3	166.35	185.869
Weight (kg.)		0.946	0	0.192	0.158
% Respect to steel			66%	79%	81%

IQAC In-charge
Rajiv Gandhi College of Engineering
Karjule Harya, Tal. Parner
Dist. Ahmednagar-414304

Principal
R G COE, Karjule Harya.

### Table 5. Comparison of Von Mises Stress in Composites

Case No.	Load	Von Mises Stress(MPa)			
		Steel Material	Glass Epoxy Material	Carbon Epoxy Material	Kevlar Epoxy Material
1.	735 N	414.20	416.00	416.10	416.41
2.	1176 N	663.40	661.30	661.70	660.19
3.	1618 N	909.50	898.70	894.10	894.16
Tensile Strength(MPa)		450	3350	3340	3350

1418

Table 6. Comparison of Factors of Safety in Composits

Case No.	Load	Factor of Safety			
		Steel	Glass Epoxy	Carbon Epoxy	Kevlar Epoxy
1.	735 N	1.11	8.31	8.29	8.30
2.	1176 N	0.70	5.22	5.21	5.23
3.	1618 N	0.51	3.84	3.85	3.86
Tensile Strength(MPa)		450	3350	3340	3350

From Table No. 2 we can observe that there is less difference in static deflection values of FEA, Analytical, and Experimental results. The static deflection is increasing with an increase in load. From Table No. 3 we can observe that there is very less difference in bending stress values which are getting by FEA, Analytical, and Experimental results. The bending stress is increasing as an increase in load with respective time in conventional steel spring. From Tables No. 4, 5, and 6 we can conclude that compared to utilizing standard steel, adopting composite material results in a material reduction of between 70 and 80 percent. It has been discovered that composite materials have a strength that is greater than that of steel. When compared to other composite materials, Kevlar is regarded as superior since it has the smallest amount of bulk while maintaining virtually the same level of strength. The tensile strength-to-weight ratio of Kevlar is greater.

V.CONCLUSION

When compared to utilizing standard steel, adopting composite material results in a material reduction of between 70 and 80 percent. It has been discovered that composite materials have a strength that is greater than that of steel. When compared to other composite materials, Kevlar is regarded as superior since it has the smallest amount of bulk while maintaining virtually the same level of strength. A very strong connection was found between the static deflection of a steel spring and the results of an analytical computation. (2-3 percent variation) The static deflection of a steel spring and the experimental deflection have been shown to have a very strong correlation (with a difference of just two to three percent). The tensile strength-to-weight ratio of Kevlar is greater.

BIBLIOGRAPHY

[1]. Balaguru, I., Anbu, G., Bhuvanesh, M., & Jayanth, N. (2016). An Overview of Design and Development of Fiber Reinforced Polymer Composite Coiled Spring for Automobile Applications. *In International Conference on Systems, Science, Control, Communication, Engineering and Technology* (Vol. 2, pp. 331-335).

[2]. Budan, D. A., & Manjunatha, T. S. (2010). Investigation on the feasibility of composite coil spring for automotive applications. *International Journal of Mechanical and Mechatronics Engineering*, 4(10), 1035- 1039.

[3]. Choi, B. L., & Choi, B. H. (2015). Numerical method for optimizing design variables of carbon-fiber- reinforced epoxy composite coil springs. *Composites Part B: Engineering*, 82, 42-49.

[4]. Kaoua, S. A., Taibi, K., Benghanem, N., Azouaoui, K., & Azzaz, M. (2011). Numerical modelling of twin helical spring under tensile loading. *Applied Mathematical Modelling*, 35(3), 1378-1387.

[5]. Michalczyk, K. (2013). Analysis of the influence of elastomeric layer on helical spring stresses in longitudinal resonance

eISSN 1303-5150

IQAC In charge
Rajiv Gandhi College of Engineering
Karjule Harya, Tal. Pamer
Dist. Ahmednagar-414304

www.neuroquantology.com

Principal
R G COE, Karjule Harya.

vibration conditions. *Archives of civil and mechanical engineering*, 13(1), 21-26.

[6]. Pyttel, B., Brunner, I., Kaiser, B., Berger, C., & Mahendran, M. (2014). Fatigue behaviour of helical compression springs at a very high number of cycles–Investigation of various influences. *International journal of fatigue*, 60, 101-109.

[7]. Skewis, W. H. (2017). Failure modes of mechanical springs. Support Systems Technology Corporation.

[8]. Sudheer, M., Pradyoth, K. R., & Somayaji, S. (2015). Analytical and numerical validation of epoxy/glass structural composites for elastic models. *American Journal of Materials Science*, 5(3C), 162-168.

[9]. Sujit, S. P., Subodh, K., & Shubham, S. (2016). Comparative study of helical compression suspension spring for different materials. Asian Journal of Engineering and Applied Technology, 5(2), 22-28.

[10]. Wang, F. (2001). Design and synthesis of active and passive vehicle suspensions (Doctoral dissertation, University of Cambridge).

1419

Source details

Feedback >   Compare sources >

European Chemical Bulletin

Open Access ⓘ

Scopus coverage years: from 2017 to Present

Publisher: Deuton-X Ltd.

E-ISSN: 2063-5346

Subject area: (Chemistry: General Chemistry)

Source type: Journal

CiteScore 2022
1.6

SJR 2022
0.247

SNIP 2022
0.471

📄 Save to source list   Source Homepage

CiteScore   CiteScore rank & trend   Scopus content coverage

ⓘ   Improved CiteScore methodology   ✕

CiteScore 2022 counts the citations received in 2019-2022 to articles, reviews, conference papers, book chapters and data papers published in 2019-2022, and divides this by the number of publications published in 2019-2022.   Learn more >

PARAMETRIC OPTIMIZATION OF ELECTROCHEMICAL MACHINING PROCESS FOR HARD HSSM2 MATERIAL (62-64 HRC) USING MINITAB TOOL

Dr. Krupal Prabhakar Pawar[1]*, Dr. Vishwajit Bhagwat[2]
Dr.Sachin Solanke[3]

Abstract

Electrochemical machining, often known as ECM, is a non-conventional machining method that is typically used for the machining of materials that are notoriously tough to work with, including super alloys, Ti-alloys, stainless steel, alloy steel, and many more. The fact that the work piece must have a nature that is electrically conductive is the most important criterion of the procedure. Both the material removal rate (MRR) and surface roughness (SR) of the components generated by ECM are influenced by a vast variety of different factors. In most cases, tool manufacturers will consult machine manuals and apply thumb rules in order to determine which parameters of the process should be optimised. In this work, Taguchi Methodology is used to investigate the influence that four significant factors have on MRR and SR for HSS M2 Hard Material (62-64 HRC). These parameters are the current, the voltage, the flow rate of electrolyte, and the inter-electrode gap. MINITAB tool is used to implement Taguchi Methodology. It is concluded that MRR and SR both values for ECM machining of HSS M2 hard (i.e. 62-64 HRC) material highly influenced by Current and Voltage parameters of ECM machine. The study is also shows that shows that Current: 280A, Voltage:36V, Flow rate: 5 m^3/min, IEG: 0.1 mm is optimum set of ECM parameters at which we get the optimum MRR i.e. 3.06 mg/min and Current: 200A, Voltage:20V, Flow rate: 9 m^3/min, IEG: 0.5 mm is optimum set of ECM parameters at which we get the optimum SR i.e. 1.93 mg/min.

[1]*Vice Principal & Assistant Professor, Department of Mechanical Engineering, RGCOE, Karjule Harya, Email:krupalpawar@gmail.com
[2]Assistant Professor, Department of Automobile Engineering, Dhole Patil College of Engineering, Pune.
[3]Assistant Professor, Department of General Engineering, Institute of Chemical Technology, Mumbai.

Corresponding Author: Dr. Krupal Prabhakar Pawar

IQAC In charge
Rajiv Gandhi College of Engineering
Karjule Harya, Tal. Parner
Dist. Ahmednagar-414304

Principal
R G COE, Karjule Harya.

Eur. Chem. Bull. 2023, 12 (S3), 6358 – 6365

6358

1. Introduction

Electrochemical machining (ECM) is a method of removing metal by an electrochemical process. It is normally used for mass production and is used for working extremely hard materials or materials that are difficult to machine using conventional methods. [1] Its use is limited to electrically conductive materials. ECM can cut small or odd-shaped angles, intricate contours or cavities in hard and exotic metals, such as titanium aluminides, Inconel, Waspaloy, and high nickel, cobalt, and rhenium alloys. [2] Both external and internal geometries can be machined. ECM is often characterized as "reverse electroplating", in that it removes material instead of adding it.[2] It is similar in concept to electrical discharge machining (EDM) in that a high current is passed between an electrode and the part, through an electrolytic material removal process having a negatively charged electrode (cathode), a conductive fluid (electrolyte), and a conductive workpiece (anode); however, in ECM there is no tool wear.[1] The ECM cutting tool is guided along the desired path close to the work but without touching the piece. Unlike EDM, however, no sparks are created. High metal removal rates are possible with ECM, with no thermal or mechanical stresses being transferred to the part, and mirror surface finishes can be achieved.

In the ECM process, a cathode (tool) is advanced into an anode (workpiece). The pressurized electrolyte is injected at a set temperature to the area being cut. The feed rate is the same as the rate of "liquefication" of the material. The gap between the tool and the workpiece varies within 80–800 micrometers (0.003–0.030 in.) [1] As electrons cross the gap, material from the workpiece is dissolved, as the tool forms the desired shape in the workpiece. The electrolytic fluid carries away the metal hydroxide formed in the process. [2] Electrochemical machining, as a technological method, originated from the process of electrolytic polishing offered already in 1911 by a Russian Chemist E. Shpitalsky. [3] As far back as 1929, an experimental ECM process was developed by W.Gussef, although it was 1959 before a commercial process was established by the Anocut Engineering Company. B.R. and J.I. Lazarenko are also credited with proposing the use of electrolysis for metal removal. [2] Much research was done in the 1960s and 1970s, particularly in the gas turbine industry. The rise of EDM in the same period slowed ECM research in the west, although work continued behind the Iron Curtain. The original problems of poor dimensional accuracy and environmentally polluting waste have largely been overcome, although the process remains a niche technique. The ECM process is most widely used to produce complicated shapes such as turbine blades with good surface finish in difficult to machine materials. It is also widely and effectively used as a deburring process. [2] In deburring, ECM removes metal projections left from the machining process, and so dulls sharp edges. This process is fast and often more convenient than the conventional methods of deburring by hand or non-traditional machining processes. [1]

According to Faraday 's law of electrolysis, if an electrode and work piece are placed in an electrolyte bath and a potential difference is applied, metal molecules from anode ionize to lose electrons and break free of the work piece, and travel through the electrolyte to cathode.

Mathematically, $m = Ite/F$ (Eq.1)

where, m = weight (g) of a material
     I = current (A)

IQAC In-charge
Rajiv Gandhi College of Engineering
Karjule Harya, Tal. Parner
. Ahmednagar-414304
Eur. Chem. Bull. 2023, 12 (S3), 6358 – 6365

Principal
R G COE, Karjule Harva.

6359

t = time (sec)

e = gram equivalent weight of material

F = Faraday's constant of proportionality (=96500 coulomb)

Practically, ECM parts are subjected to less amount of thermal stress (as the operating temperature is low) or mechanical stress (as ideally no contact occurs between tool and work piece during machining) but in real practice sparks occur which is to be avoided to minimize the tool wear. ECM process is primarily used for manufacturing components of complex shape used in aerospace and defense industries, offshore petroleum industries and medical engineering.

1. Experimental Procedure

A. Experimental Setup

The experimental trails are conducted on the ECM Machine supplied by the Metatech Industry. The set up consists of three major sub systems:

1. Machining Cell
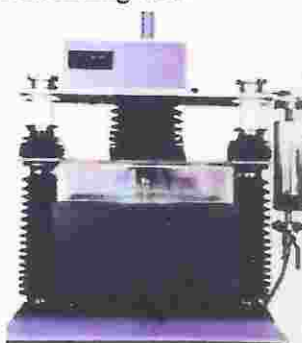
Figure 1. ECM Unit.

Figure 2. ECM Vice with Workpice.

This electromechanical assembly consists of a sturdy structure that is associated with precision machined components, servo motorised vertical up / down movement of tool, an electrolyte dispensing arrangement, illuminated machining chamber with see through window, job fixing vice, job table lifting mechanism, and sturdy stand. In order to prevent corrosion, each and every exposed component and part has been

2. Control Panel

properly coated or plated, and the appropriate material has been chosen. [4]

Technical Specification:

- Tool area - 30 mm2.
- Cross head stroke - 150 mm.
- Job holder - 100 mm opening X 50 mm depth X 100 mm width.
- Tool Feed motor - DC Servo type.

Figure 3. ECM Control Panel.

Eur. Chem. Bull. 2023, 12 (S3), 6358 – 6365

6360

The power supply is an excellent example of the seamless integration of high-current electrical, power electronics, and precision programmable microcontroller-based technologies. Because of the very low voltage at which the machine functions, there is absolutely no risk of receiving an electric shock while it is in use. [4]

Technical Specification:
- Electrical Out Put Rating - 0-300 Amps. DC at any voltage from 0 - 20 V.
- Efficiency - Better than 80% at partial & full load condition.
- Power Factor - Better than 85.
- Protections - Over load, Short circuit, Single phasing.
- Operation Modes - Manual / Automatic.
- Timer - 0 - 99.9 min.
- Tool Feed - 0.2 to 2 mm / min.
- Z Axis Control - Forward, reverse, auto forward / reverse, through micro controller.
- Supply - 415 v +/- 10%, 3 phase AC, 50 Hz.

3. Electrolyte Circulation

Figure 4. Electrolyte Circulation.

The electrolyte is pumped from a tank that has a coating that prevents corrosion with the assistance of a pump that is resistant to corrosion, and it is then supplied to the job. Electrolyte that has been used up will be poured back into the tank. The hydroxide sludge that forms will eventually fall to the bottom of the tank, where it may be drained away with little effort. The flow control valve will be responsible for controlling the electrolyte supply. The tank receives any additional electrolyte flow that is by-passed. The reservoir has distinct compartments for settling and syphoning processes. Every fitting is made of a material that is resistant to corrosion or, if required, stainless steel. [4]

B. Selection of workpiece, tool material, and electrolyte

Cylindrical blank of 30 mm diameter and 50 mm height made of HSS M2 material with high degree of hardness 62-64 HRC is selected as work piece. Tool is made of copper. 10 % NaCl along with 0.2% H_2O_2 is chosen as electrolyte such that no deposition occurs on the cathode. Unwanted machining due to stray current can be avoided on application of epoxy powder resin coating on the tool except the base of the tool.

C. Selection of machining parameters and their levels

In this experiment, four process parameters such as current, applied voltage, flow rate, inter-electrode gap (IEG) are considered as input parameters. The gap between the two electrodes (tool and workpiece) is called IEG. As the IEG decreases, current density

Eur. Chem. Bull. 2023, 12 (S3), 6358 – 6365

6361

increases and vice versa. The actual values of parameters are given in Table 1.

Table 1. Electrochemical Machining Parameters with their Levels.

Process Parameter(Unit)	Symbol	Levels		
Current(A)	A	200	240	280
Voltage(V)	B	20	28	36
Flow Rate(m³/min)	C	5	7	9
IEG(mm)	D	0.1	0.3	0.5

D. Taguchi Methodology

Taguchi methodology is the oldest and accepted industrial method of optimization. It is a powerful tool for design high quality system. It follows systematic, simple and efficient approach to optimize designs for performance, quality and cost. Taguchi method is effective method for designing process that operates reliably and optimally over a variety of conditions. To determine the best design, it requires the use of a designed experiment. Taguchi converts the objective function values to Signal-to-Noise ratio (S/N ratio) to measure the performance characteristics of the levels of control factors. In the present work experiment is designed using Taguchi technique, which uses an orthogonal matrix to study the entire parametric space with a limited number of experiments. [5]

1. Smaller is better: Condition for SR

$$S/N = -10 \times log(\Sigma(Y^2)/n)) \qquad \text{(Eq.2.)}$$

2. Larger is better: Condition for MRR

$$S/N = -10 \times log(\Sigma(1/Y^2)/n) \qquad \text{(Eq. 3.)}$$

Table 2. Design of Experiments using ECM parameters and respective response signals.

Current (A)	Voltage (V)	Flow Rate (m³/min)	IEG (mm)	MRR (mg/min)	SR (μm)
200	20	5	0.1	2.57	2.00
200	20	5	0.1	2.56	2.10
200	20	5	0.1	2.58	2.00
200	28	7	0.3	2.55	2.10
200	28	7	0.3	2.53	2.11
200	28	7	0.3	2.55	2.15
200	36	9	0.5	2.58	2.00
200	36	9	0.5	2.59	2.10
200	36	9	0.5	2.58	2.00
240	20	7	0.5	2.52	2.00
240	20	7	0.5	2.51	2.10
240	20	7	0.5	2.50	2.12
240	28	9	0.1	2.65	2.10
240	28	9	0.1	2.62	2.00
240	28	9	0.1	2.61	2.18
240	36	5	0.3	2.71	2.20
240	36	5	0.3	2.72	2.10

6362

IQAC In-charge
Rajiv Gandhi College of Engineering
Karjule Harya, Tal. Parner
Dist. Ahmednagar-414304

Principal
R G COE, Karjule Harya.

240	36	5	0.3	2.71	2.21
280	20	9	0.3	2.92	2.31
280	20	9	0.3	2.91	2.32
280	20	9	0.3	2.90	2.33
280	28	5	0.5	2.87	2.32
280	28	5	0.5	2.86	2.30
280	28	5	0.5	2.87	2.31
280	36	7	0.1	3.05	2.50
280	36	7	0.1	3.06	2.52
280	36	7	0.1	3.04	2.51

2. Results and Discussions

2.1 Results and Discussion for MRR
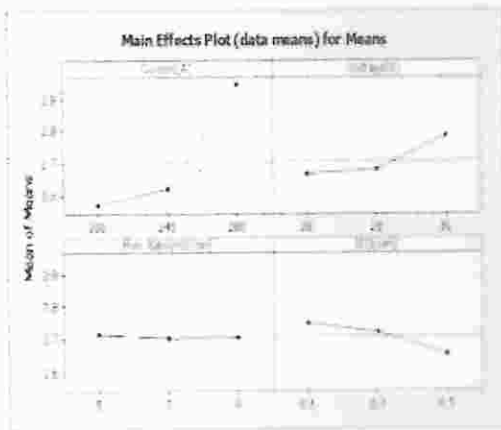
Graph No. 1 Main Effect Plot for Means of MRR.
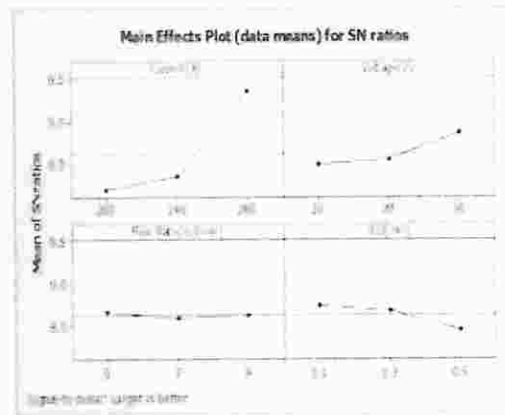
Graph No. 2 Main Effect Plot for SN ratios of MRR.

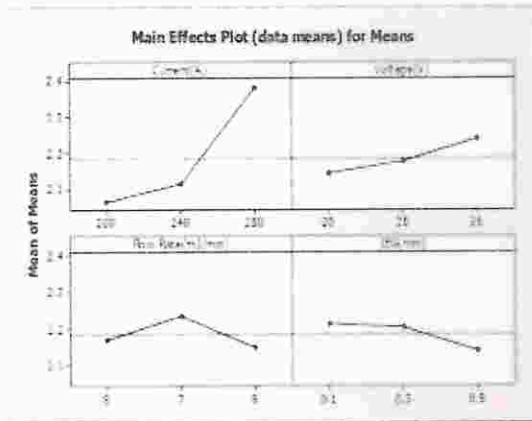Graph 1 shows that material removal rate (MRR) for ECM machining for HSS M2 hard material is increased with increase in current(A) values and also MRR is increased with increase in voltage (V) values. MRR is slightly decreased with increased in flow rate of electrolyte and slightly increases with decreases in flow rate of electrolyte. MRR is decreased with increase in Inter-electrode gap(IEG). Graph 2 shows that Current: 280A, Voltage:36V, Flow rate: 5 m³/min, IEG: 0.1 mm is optimum set of ECM parameters at which we get the optimum MRR which is 3.06 mg/min. The response tables 3 and 4 shows that MRR is more influenced by current (Rank:1) and then voltage(Rank:2).
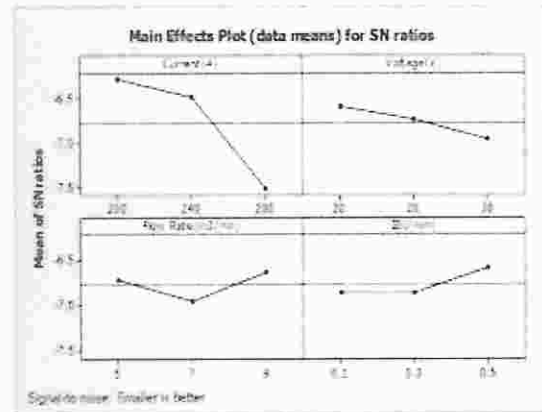
Table 3. Response Table for S/N ratios (Larger is better)

Level	Current(A)	Voltage (V)	Flow Rate (m3/min)	IEG (mm)
1	8.193	8.490	8.672	8.757
2	8.350	8.549	8.596	8.685
3	9.370	8.866	8.636	8.461
Delta	1.167	0.377	0.076	0.296
Rank	1	2	4	3

Table 4. Response Table for Means of MRR

Level	Current(A)	Voltage (V)	Flow Rate (m3/min)	IEG (mm)
1	2.566	2.663	2.717	2.749
2	2.617	2.679	2.701	2.722
3	2.942	2.782	2.707	2.663
Delta	0.377	0.119	0.016	0.096
Rank	1	2	4	3

Eur. Chem. Bull. 2023, 12 (S3), 6358 – 6365

6363

2.2 Results and Discussion for SR

Graph No. 3 Main Effect Plot for Means of SR

Graph No. 4 Main Effect Plot for SN ratios of SR

Graph 1 shows that surface roughness (SR) for ECM machining for HSS M2 hard material is increased with increase in current(A) values and also SR is increased with increase in voltage (V) values. SR is increased up to 7 m^3/min in flow rate of electrolyte and then decreased. SR is decreased with increase in Inter-electrode gap(IEG). Graph 2 shows that Current: 200A, Voltage:20V, Flow rate: 9 m^3/min, IEG: 0.5 mm is optimum set of ECM parameters at which we get the optimum SR which is 1.93 mg/min. The response tables 5 and 6 shows that SR is more influenced by current (Rank:1) and then voltage(Rank:2).

Table 5. Response Table for S/N ratios (Smaller is better)

Level	Current (A)	Voltage (V)	Flow Rate (m3/min)	IEG (mm)
1	-6.287	-6.604	-6.723	-6.961
2	-6.497	-6.741	-6.952	-6.856
3	-7.525	-6.964	-6.633	-6.592
Delta	1.238	0.360	0.319	0.269
Rank	1	2	3	4

Table 6. Response Table for Means of SR

Level	Current (A)	Voltage (V)	Flow Rate (m3/min)	IEG (mm)
1	2.063	2.142	2.171	2.212
2	2.112	2.174	2.234	2.202
3	2.380	2.238	2.149	2.139
Delta	0.318	0.096	0.086	0.073
Rank	1	2	3	4

3. Conclusion

From above investigation, it is concluded that MRR and SR both values for ECM machining of HSS M2 hard (i.e. 62-64 HRC) material highly influenced by Current and Voltage parameters of ECM machine. The study is also shows that shows that Current: 280A, Voltage:36V, Flow rate: 5 m^3/min, IEG: 0.1 mm is optimum set of ECM parameters at which we get the optimum MRR i.e. 3.06 mg/min and Current: 200A, Voltage:20V, Flow rate: 9 m^3/min, IEG: 0.5 mm is optimum set of ECM parameters at which we get the optimum SR i.e. 1.93 mg/min. In order to validate the results obtained, there are three confirmation experiments conducted for each of the response characteristics (MRR, Ra) at optimal levels of the process variables and at initial levels of process variables. The average values of the optimum characteristics at initial levels, predicted value levels and experimental value levels are obtained.

4. References

1. Todd, H. Robert; Allen, K. Dell; Alting, Leo (1994), Manufacturing Processes Reference Guide (1st ed.), Industrial Press Inc., pp. 198–199, ISBN 0-8311-3049-0.
2. Valenti, Michael, "Making the Cut." Mechanical Engineering, American Society of Mechanical Engineers,2001.http://www.memagazine.org/backissues/membersonly/nov01/features/makcut/makcut.html Archived 2010-07-05 at the Wayback Machine accessed 2/23/2010.
3. http://electrochemicalmachining.com/technology/process-history.
4. http://metatechind.com/html/ecm.htm#Industrial%20Setups.
5. Pawar, K.P., & Palhade, R.D. (2015). Multi-objective Optimization of CNC Turning Process Parameters for High Speed Steel (M2) Using Taguchi and ANOVA Method. International Journal of Hybrid Information Technology, 8, 67-80.
6. Acharya, B.G., Jain, V.K., Batra, J.L., 1986. Multi-objective optimization of ECM process, Precision Engineering, 8(2), p.88-96.
7. Jain. N. K., Jain, V.K., 2007. Optimization of electro-chemical machining process parameters using genetic algorithms, Machining Science and Technology, 11, p.235-258.
8. Asokan, P., Kumar, R. Ravi, Jeyapaul, R., Santhi, M., 2008. Development of multi-objective optimization models for electrochemical machining process, Int. J. Adv. Manuf. Technol., 39, p.55-63.
9. Chakradhar, D., Venu Gopal, A., 2011. Multi-Objective Optimization of Electrochemical machining of EN31 steel by Grey Relational Analysis, International Journal of Modeling and Optimization I(2).

IQAC In-charge
Rajiv Gandhi College of Engineering
Karjule Harya, Tal. Parner
Dist. Ahmednagar-414304

Principal
R G COE, Karjule Harya.

Optimization of Burnishing Process to Improve Surface Finish Using Taguchi Methodology

Dr. Krupal Prabhakar Pawar[1*]

Associate Professor, Mechanical Engg. Department,Rajiv Gandhi College of Engineering,Karjule Harya[1]
Email:krupalpawar@gmail.com

Abstract

In the current paper, the Taguchi Method is applied to improve the surface finish of the Aluminum Alloy 5083. The three machining parameters such as spindle speed, feed, and depth of cut are selected for the study. L9 orthogonal array is selected for the design of experiment. Surface finish is chosen as quality characteristic or response parameter. All trials are done in the dry environment. After conducting the experiment, we have found the optimum set of machining parameters at which we get minimum surface roughness means we get the best surface finish. The optimum level of parameters is A3, B3, and C1. (i.e. 650 rev/min, 0.035 mm/rev,0.08mm). The optimum value of surface roughness predicted by MINITAB 21.1 software at optimum levels of machining parameters is 0.67 um.

5880

1. INTRODUCTION

The surface quality of the component is an important factor in determining how long it will last. After machining, a component will have machining marks if the procedure was a turning, milling, or drilling operation. Because they lower the component's strength, machining marks are almost never something that should be desired, regardless of the purpose, they are being used for. There are many other procedures for improving the surface, such as honing, lapping, grinding, and so on. The surface finishing of the component is significantly improved as a result of all of these operations. However, just improving a component's surface polish will not make it last longer. It is necessary to enhance the "Surface Integrity" in order to prolong the useful life of the component. Surface finishing processes, such as shot peening, low plasticity burnishing, burnishing, and other similar processes, are examples of cold working-surface treatment processes. During these processes, plastic deformation of surface irregularities occurs as a result of applying pressure to a surface in order to generate a uniform and work-hardened surface, which improves Surface Integrity (SI). In this particular piece of study, the flank face of the turning tool is used within the context of a finishing tool. Because of its widespread use in the aerospace and shipbuilding industries, Aluminium Alloy 5083 was chosen for this investigation. It has a low density and high thermal conductivity which are characteristics shared by all aluminium alloys.
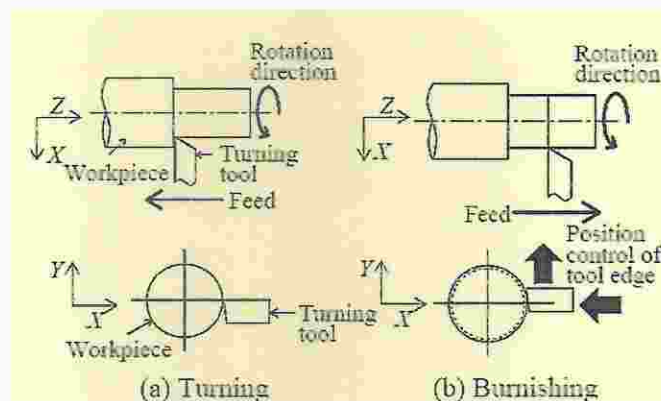

Figure1. Schematic of a burnishing method utilizing flank face of tool nose

2. LITERATURE SURVEY

Lv Jinlong et al. [1] "studied the effect of burnishing on grain texture and oxidative behavior of 2024 aluminum alloy. They used the material 2024-T3. The length & the radius of the workpiece samples were 200 mm and 46 mm, respectively. The burnishing process was performed with the help of a cylindrical-ended PCD (Polycrystalline diamond) tool; with roll diameter and length of the PCD tool were 2 mm and 3 mm, respectively. The tool's rotating speed was 3000 rpm. The burnishing depth was 20 μm and 30 μm, respectively. The electron backscattered diffraction (EBSD) scans were conducted for an Electrochemical measure of surface quality after burnishing. They got results as improved corrosion property was due to positive grain modification of the burnished surface."

El-Tayeb et al.[2] "found the influence of roller burnishing contact width and burnishing orientation on surface quality and tribological behavior of Aluminum 6061. In this study, Aluminum 6061 was used as workpiece material, and carbon chromium rollers with different roller contact widths (such as 1, 1.5, and 2mm) were used in a burnishing tool with an exchangeable adapter for ball and roller for the purpose of the experimental tests. They found best possible ranges for burnishing speed & forces are to be 250-420 rpm for 1mm roller contact thickness. They found burnishing with smaller roller contact width (1mm) is capable of improving the surface roughness by up to 40%. They also found that the burnishing force above 220N is capable of decreasing the surface roughness by 35%. The authors have found that the coefficient of friction of burnished surfaces is dependent on the surface roughness. A low friction coefficient corresponds to low surface roughness. In this study the SEM examination of the damaged surface reveals that interposing lubricant during Tribo-test acts as a cooler and polishing agent, resulting in a smoother surface compared to the burnished surface. Under dry contact conditions, a burnished surface using smaller roller contact width produces the lowest friction coefficient. An increasing burnishing force beyond a particular limit has a harmful impact on the wear resistance of burnished Aluminum 6061 surfaces."

U.M. Shirsat et al. [3] "studied the parametric analysis of the combined turning and ball burnishing process on al alloy. They had selected the Al-alloy as their working material. In this experiment, twelve tests were carried out at these levels. For each block, the model equations for surface roughness and surface hardness are obtained by using the analysis of variance technique, F-test, and regression coefficient. The authors also worked on the parametric analysis of the combined turning and ball burnishing process. After the results, they concluded that the micro-hardness increased with force up to a certain extent only."

P N. Patel et al. [4] "optimized burnishing process parameters for improving the surface hardness of Aluminum Alloy 6061. They selected their workpiece and tool material as Al-alloy 6061 and high chromium high carbon with 8 mm diameter. They got the optimum parameters for hardness as burnishing speed as 250 RPM, feed as 0.06 mm/rev, force as 8 Kgf, and no. of passes as 5. The authors used the Taguchi method for their analysis purpose. They found that as speed increases the surface hardness increases and if there is a further increase in speed then hardness decreases. They also concluded that when the feed rate was low the distance between successive traces was small."

Fathi Gharbi et al. [5] "studied ductility enhancement of aluminum 1050A rolled sheet with a newly designed ball burnishing tool device. They received workpiece material in a form of cold-rolled plates with a thickness of 3 mm. Selected material has huge scope in the manufacturing industry. They observed that an increase in the burnishing speed, the feed, or the force causes a decrease in mean roughness down to a minimum value. After crossing this minimum value, the mean roughness starts to increase with the increase of each of the burnishing parameters. The optimal feed rate and burnishing force for aluminum 1050A plates are 0.1 mm/rev and 100 N, resp. They also got the lowest values of surface roughness at a feed rate ranging from 0.1 to 0.15 mm/rev."

Amit Patel et al. [6] "studied the effect evaluation of the roller burnishing process on the surface roughness of 6061 T6 al alloy using response surface methodology. Response surface methodology was employed to analyze the effect of parameters to ensure a minimum surface roughness. The authors used the ANOVA model

5881

for the analysis of their study. The usefulness of roller burnishing decreases with an increase in feed rate. Surface roughness is increased with an increase in no. of passes, best results were obtained with lower feed 0.06 mm/rev. They suggested that for better results prefer the force of 15-20 kg with the four number of passes."

El-Axir, Othman,et al. [7] "considered the improvements in beyond-roundness and micro-hardness of inner surfaces by the internal ball burnishing process. They used Al-alloy 2014 workpiece and carbon-chromium steel balls as a tool. They concluded that if there is an increase in burnishing speed then it will lead to a considerable reduction in beyond-roundness; though, it has no significant effect on surface microhardness. The suggested burnishing feed that results in high surface microhardness and a considerable reduction in beyond-roundness is in the range of 0.2 to 0.35 mm/rev. In the same study, they got the best results for surface microhardness at depth of penetration in the range from 0.025 to 0.045mm, whereas the beyond-roundness is obtained when applying a high depth of penetration. A simple and adequate experimental design, response surface methodology (RSM), with the Box and Hunter method was used to investigate the effect of the burnishing process parameters."

J. A. Travieso, et al.[8] "studied improving the surface finish of concave and convex surface using a ball burnishing process. They used the workpiece with the concave and convex surface of the two different materials as aluminium A92017 and steel G10380. Both workpiece materials are composed of three areas in which there are three curves of 50, 100, and 50 mm of diameter resp. Al A92017 with a convex surface with a radius between 50 and 100mm, the burnishing process helps to improve the surface roughness. Steel G10380 with a convex surface with a radius between 50 and 100mm, the burnishing process will again help to improve the surface roughness. There is a specific prediction for Al A92017; better results can be achieved with a smaller radius in convex surfaces and with a higher radius in concave surfaces."

M. R. Stalin John et al. [9] "investigated the effect of the roller burnishing process on Al 63400 material. Their burnishing tool was with interchangeable springs, designed and fabricated for experimentation. An interchangeable spring was designed to give a load up to 1430 N. The authors used response surface methodology for their analysis. The optimization is carried out on the surface which already has a surface roughness of 0.145μm and a surface hardness of 43 HRB. The optimized surface characteristics are studied for the parameters burnishing force 1200 N, feed 200 mm/min, step over 3 mm, and no. of passes 2. The analysis of Al 63400 was done on a computer numerical control vertical machining center. The surface characteristics obtained were surface roughness 0.141μm and surface hardness 44 HRB."

P. Saritha [10] "states that the roller burnishing process is used to get a good surface finish for material such as aluminium & mild steel. The contact analysis proves about a 10-15% variation in results. Their results obtained for contact stresses in a roller burnishing process were found using different theories and numerical methods. The best approach is to adopt multi-scale FEM methods."

Shailesh Dadmal et al. [11] "studied finite element analysis of the burnishing process. Surface finish has a long-drawn-out effect on almost every material. They evaluated the consequences of burnishing parameters along with the surface integrity before the actual functioning. They presented the process of developing the 2D model using transient structural analysis of the roller burnishing process. The material of the roller in the roller tool was tool steel and high carbon high chromium steel. They found that the results of the FEA are coinciding with the experimental results with less than 10% error."

D. M. Mate et al. [12] "formulated a mathematical model for Al-2014 with a spherical surface burnishing tool. The authors are dealing with the effect of the burnishing process on the aluminium alloy 2014. The authors say that it is essential to correlate quantitatively various independent and dependent terms involved in this very intricate phenomenon. This correlation is nothing but a mathematical model as a design tool for such a situation. The author's objective behind this was to minimize processing torque; energy and time with the constraints involved were bound values of π terms. The author's formulated LPP on the basis of the computed results. The computed result on the basis of dimensional analysis provides effective guidelines to manufacturing engineering so that they can minimize E, Ra, and t for higher performances."

Kunal R. Patel et al. [13] "studied the

5882

investigation of roller burnishing process parameters on the surface roughness of Al-Alloy 6351 T6 by the response surface methodology. Response Surface Methodology is a collection of mathematical and statistical techniques that are useful for modeling and analysis of process parameters and optimization of response. They got the results as follows: the minimum surface roughness value 0.080μm was obtained at values of 450 rpm speed, feed rate 0.064 mm/rev, no. of tool passes 4, interference 2 mm. In this investigation, the experimental design was established on the basis of 2k factorial, where k is the number of variables, with central composit1e-second-order rotatable design to improve the reliability of results and to reduce the size of experimentation without loss of accuracy."

Manabu Iwai et al. [14] "studied the development of a new burnishing method utilizing a flank face of a turning tool and its burnishing performance. The authors had introduced, a new method using a flank face situated in a few millimeters lower part of the nose cutting edge of a tool. The workpiece material used was carbon steel (S45C) of φ30mm and the turning insert was used as the face of the tool nose."

By studying various papers, it is concluded that no work is found for optimizing the burnishing process by Taguchi Method for Aluminum Alloy 5083. In the present work, we are focusing on the optimization of burnishing process parameters for optimum surface finish.

2. EXPERIMENTATION SETUP AND CUTTING CONDITIONS

For the conducting experimental trials, the ACE make CNC model Simple Turn-5075 Siemens 802C is employed (see Figure.1). First of all, it is very important to select a process with process parameters and their levels. In the research work, machining parameters such as spindle speed, feed, and depth of cut are selected for optimization of surface finish.The surface finish is measured with a Mitutoyo surface roughness tester. In the present research work, we are going to utilize the Taguchi method for experiment design.The design of the experiment is done with help of MINITAB 21.1 software and for this condition suited orthogonal array such as L9 is selected from the series of arrays.The design of experimental trials is shown in Table 2.Aluminium Alloy 5083 material rods with 50 mm diameter and 300 mm length are selected for experimental trials. In the present work, a rectangular shape TNMG 160408 insertis used as a cutting tool used for Aluminium Alloy 5083 materialspecimens. The clearance angle of the selected insert is zero. The inscribed circle size is 9.5mm and the thickness is 5mm. A tool holder such as PCLNR 2525M12 is employed to hold the insert.

5883

Figure 1. Experimental Unit

Figure 2. Surface Roughness Tester

Table 1. Control Factors with Levels

Levels	Control Parameters		
	Spindle Speed (Rev/min)	Feed Rate (mm/rev)	Depth of Cut (mm)
L1	850	0.045	0.08
L2	750	0.040	0.06
L3	650	0.035	0.04

After DOE, it is important to conduct all trials as per the design of the experiment.After inserting surface roughness values in the MINITAB 21.2 software, the signal-to-noise ratios for each trial are calculated by applying the smaller is better condition.

5884

$$S/N = -10 \times log(\Sigma(Y^2)/n)) \text{ Eq. (1)}$$

Where, S/N-Signal to Noise Ratio, Yi – i[th] observed value of the response, n - Number of observations in a trial, Y - Average of observed responses values.

Table 2. Experiment Conductionas DOE

Spindle Speed Rev/min	Feed (mm/rev)	Depth of Cut (mm)	Surface Roughness (Ra) in μm	S/N Ratio
850	0.045	0.08	1.20	-1.58362
850	0.040	0.06	0.76	2.38373
850	0.035	0.04	0.53	5.51448
750	0.045	0.06	0.91	0.81917
750	0.040	0.04	0.72	2.85335
750	0.035	0.08	0.67	3.47850
650	0.045	0.04	1.10	-0.82785
650	0.040	0.08	0.71	2.97483
650	0.035	0.06	0.62	4.15217

Table 3. Response Table for Signal-to-Noise Ratios (Smaller is better)

Level	Speed	Feed	Depth of Cut
1	2.0997	4.3817	2.5133
2	2.3837	2.7373	2.4517
3	2.1049	-0.5308	1.6232
Delta	0.2840	4.9125	0.8901
Rank	3	1	2

Table 4. Response Table for Means

Level	Speed	Feed	Depth of Cut
1	0.8100	0.6067	0.7833
2	0.7667	0.7300	0.7633
3	0.8300	1.0700	0.8600
Delta	0.0633	0.4633	0.0967
Rank	3	1	2

The calculation of signal-to-noise ratios with help of MINITAB 21.1 software is shown in the following Table 2. From Table 4 we can conclude that feed rate is the most influencing factor for the surface finish which shows rank first in the response table of means.

3. RESULTS AND DISCUSSION

The graphs are plotted using MINITAB 21.1 software. The main effect plots for means and S/N ratio are shown in Figures 3 and 4 respectively.
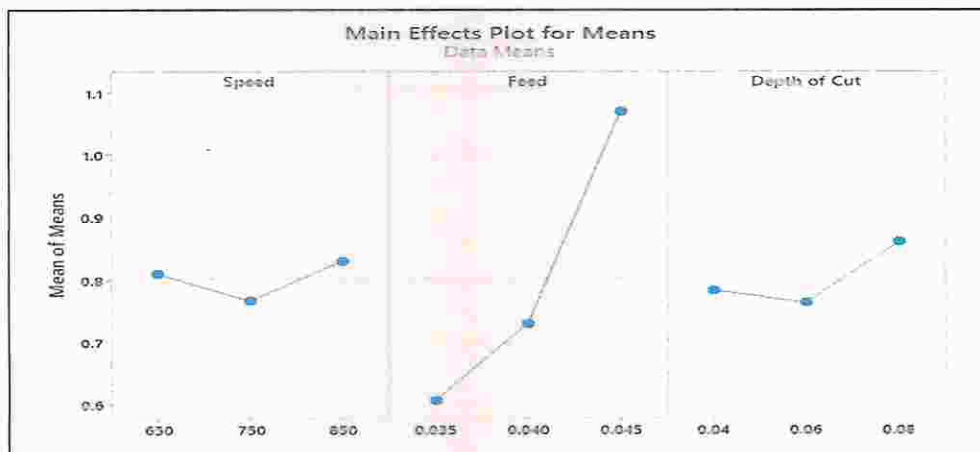
5885

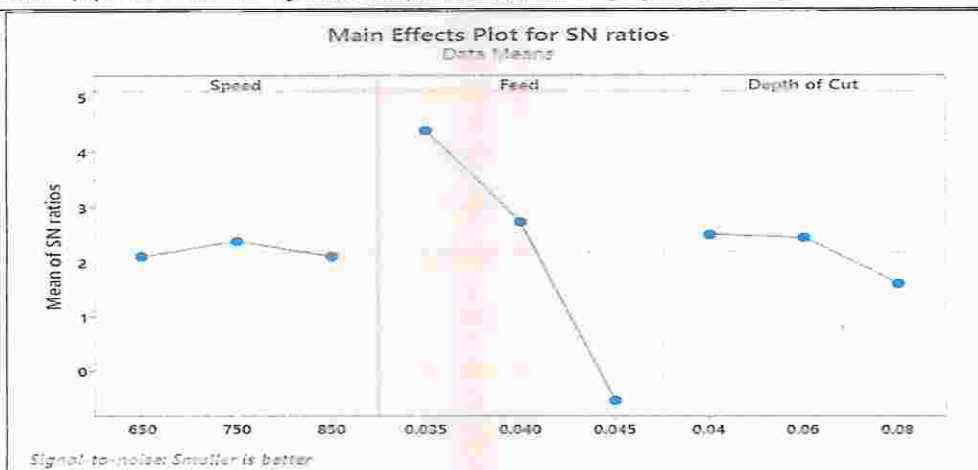Figure 3. Main Effects Plot for Means

Figure 4. Main Effects Plot for S/N Ratio

Figure 4 indicates that the optimum level of parameters is A3, B3, and C1. (i.e. 650 rev/min, 0.035 mm/rev,0.08mm). Using these parameters in the burnishing process we get the maximum surface finish. Figure 3 indicates that the surface finish first decreases with an increase in spindle speed and then increases with an increase inspindle speed. Surface finish increases with an increase in feed rate. The surface finish decreases with an increase in the depth of cut and then increases with an increase in the depth of cut.

4. VALIDATION OF RESULT

After conducting the experiment, we have found the optimum set of machining parameters at which we get minimum surface roughness means we get the best surface finish. The optimum level of parameters is A3, B3, and C1. (i.e. 650 rev/min, 0.035 mm/rev,0.08mm). The optimum value of surface roughness predicted by MINITAB 21.1 software at optimum levels of machining parameters is 0.67 μm. In this stage of validation, we have to check the repeatability of our result.

Table 5. Validation of Result

Optimum Level of Parameters	Surface Roughness Predicted by MINITAB 21.1 Software	Trials Conducted at the Optimum Level of Parameters to find the corresponding Ra value	The average value of Ra values collected after conducting Trials	Error = (Surface Roughness Predicted by MINITAB 21.1 Software) – (The average value of Ra values collected after conducting Trials)
A3, B3, and C1. (i.e. 650 rev/min, 0.035 mm/rev, 0.08mm)	0.67 μm	0.65 μm	0.65 μm	0.02
		0.62 μm		
		0.67 μm		
		0.68 μm		
		0.65 μm		

We have conducted the trials to find surface roughness values at optimum levels. we have conducted 5 validation trials as shownin Table 5. From Table 5, we can conclude that the error value is 0.02 which is within the acceptable limit. In this way conducted the validation.

5. CONCLUSION

It is concluded that the optimum set of machining parameters at which we get minimum surface roughness means we get the best surface finish.

The optimum level of parameters is A3, B3, and C1. (i.e. 650 rev/min, 0.035 mm/rev,0.08mm). The optimum value of surface roughness predicted by MINITAB 21.1 software at optimum levels of machining parameters is 0.67 μm and the actual surface finish after trials is 0.65 μm which is the average of all surface finish measured values. The difference is 0.02 μm which is minimum so the optimum parameters set is correct.

BIBLIOGRAPHY

[1] Jinlong, L., & Hongyun, L. (2013). Effect of surface burnishing on texture and corrosion behavior of 2024 aluminum alloy. Surface and Coatings Technology, 235, 513-520.

[2] El-Tayeb, N. S. M., Low, K. O., & Brevern, P. V. (2007). Influence of roller burnishing contact width and burnishing orientation on surface quality and tribological behaviour of Aluminium 6061. Journal of materials processing technology, 186(1-3), 272-278.

[3] Shirsat, U. M., & Ahuja, B. B. (2004). Parametric analysis of combined turning and ball burnishing process.

[4] Patel, P. N., Patel, N. B., & Patel, T. M. (2014). Parametric Optimization of Ball Burnishing Process Parameter for Hardness of Aluminum Alloy 6061. IOSR Journal of Engineering (IOSRJEN), 4(08), 21-26.

[5] Gharbi, F., Sghaier, S., Hamdi, H., & Benameur, T. (2012). Ductility improvement of aluminum 1050A rolled sheet by a newly designed ball burnishing tool device. The International Journal of Advanced Manufacturing Technology, 60(1), 87-99.

[6] Patel, A., Patel, D., & Banker, K. (2014). Effect evaluation of roller burnishing process on surface roughness of 6061 T6 A l alloy using response surface methodology. Int J Sci Res Dev, 8, 142-5.

[7] El-Axir, M. H., Othman, O. M., & Abodiena, A. M. (2008). Improvements in out-of-roundness and microhardness of inner surfaces by internal ball burnishing process. Journal of materials processing technology, 196(1-3), 120-128.

[8] Travieso-Rodríguez, J. A., Dessein, G., & González-Rojas, H. A. (2011). Improving the surface finish of concave and convex surfaces using a ball burnishing process. Materials and Manufacturing Processes, 26(12), 1494-1502.

[9] Stalin John, M. R., & Vinayagam, B. K. (2011). Investigation of roller burnishing process on aluminium 63400 material. Australian Journal of Mechanical Engineering, 8(1), 47-54.

[10] Ulhe, P. N., Patil, U. D., & Patil, C. R. (2019). Optimization Of Roller Burnishing Process Parameters On Surface Roughness Using Response Surface Methodology. Materials Today: Proceedings, 18, 3632-3637.

[11] Shaiesh Dadmal, Prof. Vijay Kurkute, (2017), "Finite Element Analysis of Roller Burnishing Process", Int Research J of Engg. And Technology vol. 4 Issue 6

[12] Mate, D. M., & Choudhari, P. S. (2014). Formulation of Experimental Data Based Mathematical Model for Al 2014 with Spherical Surface Burnishing Tool. International Journal of Research in Mechanical Engineering, 2(3).

[13] Nikunj, K., & Kiran, A. (2014). Parametric optimization of process parameter for roller burnishing process.

[14] Iwai, M., Hashimoto, H., & Suzuki, K. (2016). Development of a New Burnishing Method Utilizing a Flank Face of a Turning Tool and its Burnishing Performance. In Advanced Materials Research (Vol. 1136, pp. 227-232). Trans Tech Publications Ltd.

Advanced Manufacturing Process Development for Automation in the Industry using Artificial Intelligence-Based System

D. Kumaravel,
AMET University,
Chennai, Tamil Nadu, India.
kevinkumaravel@gmail.com

Prashant Tomar,
Assistant Professor,
Department of Mechanical
Engineering,
Parul Institute of Technology, Parul
University,
Vadodara, Gujarat, India,
prashantsingh.tomar@paruluniversity.a
c.in

Kodirova Dilshodkhan Tulanovna
Candidate of Technical Sciences,
Docent, Uzbekistan,
Department of Chemistry and Chemical
Technology,
Fergana Polytechnic Institute,
Fergana.
d.qodirova@ferpi.uz
0000-0003-3629-3987

Sushant Sharma
Assistant Professor,
Department Of Mechanical
Engineering, FET, MRIIRS
Manav Rachna International Institute
of Research And Studies,
Faculty of Engineering and
Technology,
sushant1.fet@mriu.edu.in

Dr. Krupal Prabhakar Pawar
Associate Professor
Mechanical Engineering
Rajiv Gandhi College Of Engineering,
India.
Krupalpawar@Gmail.Com

Dr. Pravin P Patil
Professor,
Department of Mechanical
Engineering,
Graphic Era Deemed To Be University.
Dr.Patil@Geu.Ac.In

Abstract— The record of answer books and attendance (RABA) in any examination system is an unexplained but necessary component of educational institutions to register the presence and trace the unique number of answer sheets of a certain applicant. Manually writing in the RABA of pupils traditionally is time-consuming, difficult to manage, and prone to human mistakes. To address these issues, an AI-based system with facial recognition and a fingerprint-based biometric system of digital RABA is presented. In this work, an automated system for face recognition and fingerprint identification using biometrics is proposed, and the answer sheet barcode is subsequently scanned for RABA input using a camera module. Finally, all of these records are stored in a database and may be retrieved at any moment by the institution of the university. This approach provides a faster and more precise means of avoiding proxy attendance.

Keywords: Face Recognition, Fingerprint Recognition, Barcode, RABA, RFID, Artificial Intelligence, and fixed-point pictures.

I. INTRODUCTION

Manual examination of understudies' quality in the assessment corridor amid their separate class/test hours has recently caused aggravation because of close-to-home errors. The traditional technique for participation consumes time, necessitates physical labor, and is primarily concerned with how participation may be controlled. Likewise, there is a possibility that understudies who did not respond at the involvement call may guarantee their participation later on. It is also quite tiresome for the delegate to walk around the grounds inspecting each homeroom at assessment time. As a result, there is a demand for a competent and uncomplicated

approach for truly assessing during the evil computer-based intelligence innovation can answer this issue by use of biometrics-based participation checking [1][2].

Biometrics can be physiological or social [3]. The physiological properties are contained in the real bodily part (like fingerprints, hand-shaped impressions, iris, face, DNA, hand calculation, retina, and so forth) Individuals' conduct qualities include behaviors such as dialogue acknowledgment, key output, and signature verification. Any biometric framework consists of two stages: the enrollment stage and the discovery stage. The recognition of an individual through his body, and the subsequent identification of this body with a "personality" created from the outside, creates a valid apparatus for character assessment. Thus, biometrics isn't simply an intriguing subject in model recognition research; when used correctly, it might potentially make our general population more safe, less deceptive, and more understandable. Various biometric validation frameworks have been used, but each has its own set of advantages and disadvantages depending on the quality, recording device, data set, and associated properties [4][5]. A biometric framework develops a person's personality by following a development. There is an interest in developing a powerful single-mode framework to secure protection after investigating the problems of the current identification framework. Another way for capturing involvement by perceiving face, as well as distinctive mark design, can be used to accomplish this. These two advancements are computer-based. There are several web programs available for the biometric participation framework that may be used with a mobile phone. Phones are normally not authorized to be communicated during assessment; so, biometrics (fingerprint

and face recognition) may be used in Raspberry Pi with different modules conducting facial recognition and biometrics can be connected. As a result, the architecture is compact and secure. As a result, our framework is limited since each of the extremely important units gets prepared inside a convenient handheld box.

Dhanalakshmi et al. [6] used an information base created by the organization as well as the Aadhaar Central Identification Repository (CIDR). Remote unique mark terminals are aware of capturing and storing participation records in the gadget data set and renewing them in the server data set.

Mohamed et al. [7] illustrated a model of the Class Attendance Management System (CAMS) developed with an NFC (or RFID) tag/card. The software on the NFC-enabled phone reads an understudy ID by just touching it against an NFC stu-gouge ID card. The program utilizes FC-enabled Android gadgets to read the understudy grounds card and focus his ID number to be used as an understudy identify in CAMS.

Rathod et al. [8] used Viola-Jones and HOG in addition to the SVM classifier. Scaling, illumination, obstacles, and posture should all be evaluated constantly. PSNR esteems are used to complete the quantitative examination.

Masruroh et al. [9] reviewed the related efforts in the fields of participation management, NFC, facial recognition, microcomputers, and distributed storage. They proposed a framework that reduces the amount of paper used and eliminates the time and effort used in assessing participation using a mobile-based participation paradigm.

II. Proposed Methodology

The following components are essential to the system:

- Raspberry Pi 4th Gen + 16GB SD Card
- Heat Sink and Fan
- Fingerprint Scanner, R307
- 7-inch touch display
- 20000 mAh Lithium batteries
- Pi 8 MP camera Face recognition and barcode scanning are possible with the camera module.

The entire system was written in Python and interacted with the database using Open CV modules. The attendance may be accessed straight from the database using a web-based application. To register and confirm biometric data, fingerprint detection and facial recognition algorithms are used.

The real assets or equipment prerequisites are the typical arrangements of necessities specified by every working framework or programming application, as shown in Fig. 1.

Fig. 1. Proposed System Hardware Description

Biometric participation frameworks that are generally accessible are statically located and require an individual to go toward the gadget to stamp their involvement. Perhaps the most significant negative is that the framework is huge, and because of its static area, most clients must wait their time. In this manner, an application is offered that incorporates biometric aspects (facial and finger) for the involvement of picked understudies alongside a normal tag scanner for their RABA transit in the assessment lobby. The suggested framework is small and compact.[10]

The suggested architecture has been designed with three essential procedures in mind.

1. Student and invigilator/faculty registration in the examination hall.
2. A comparison of the data entered during registration with the parameters. When a match is detected, the response sheet number is retrieved using a camera and saved as attendance, along with the date and time.
3. The student biometric information, along with the specific barcode of the scanned copy, is saved in the database and transferred to the server database.

The registration phase consists following steps-

STEP 1.   Enter the user's (faculty or student) information.

STEP 2.   Scan Your Fingerprint.

STEP 3.   Take a facial image.

STEP 4.   Extracting features from facial images and fingerprints and saving them to the database for further verification.

Face feature extraction: For face feature extraction, 2-D facial landmarks are considered. The feature distance in the face represents several extracted characteristics from the face.

The Head position characteristics did not reflect temporal information, that is, they did not transmit changes in time. As a result, the horizontal and vertical motion of particular face points, namely points 2, 4, 14, and 16, was used to assess Head Motion. The mean, median, and mode of displacement in the horizontal and vertical directions were then computed. Facial temporal information may transmit information about a person's affective state, and so there may be a correlation between them. This was implemented as face characteristics derived from the eyes, lips, brows, and head.

Fingerprint feature extraction: A fingerprint template is a collection of fingerprint features kept in a user's fingerprint database. During the enrollment process, it is saved to reflect

the true owner of the fingerprint. In a fingerprint recognition system, the matching algorithm is critical. Matching algorithms are used to compare previously stored fingerprint templates to candidate fingerprints for authentication. Pattern-based (or image-based) algorithms and Minutia Feature extraction-based algorithms are two commonly used algorithms. The fundamental fingerprint patterns (arch, whorl, and loop) of a previously stored template and a candidate fingerprint are compared using pattern-based algorithms. Other algorithms take advantage of minute details on the finger.

In this research, the Minutia Feature extraction-based technique was employed to match the fingerprint templates.

The steps in the Recognition Phase are as follows:

1. Recognize the invigilator's fingerprint and face and record their attendance.
2. Recognition of a student's fingerprint and face to record attendance.
3. Scan the answer sheet's barcode.

III. RESULT

The suggested system was developed, and testing was carried out in Python. Figures 4–8 show screenshots of the implemented model.

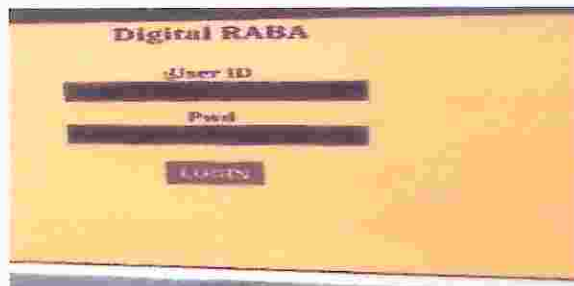Fig. 2. Home page

GUI of the home page as shown in Fig. 4

Fig. 3. Institute Login

The institute's login page is seen in Fig. 5. An authorized user can register both students and instructors after matching credentials. Biometrics (fingerprints and faces) are recorded and kept in a database.

Figure 6 depicts the biometric recognition page. There is a link on this page for both faculty and students. When "Student biometrics" is selected, the face and fingerprint are collected and compared to all traits in the database. If any of the characteristics (fingerprint or face) match (fig. 7), the scanning of the response sheet barcode will be redirected (fig. 8). The scanned answer sheet number, together with the date

and time, is saved in the database. This would keep track of the student's attendance. Otherwise, the message "Biometric Mismatch" will appear. If the biometrics match was unsuccessful for whatever reason, or if the student's information is not in the database, manual input is an alternative. When "Faculty biometrics" is selected, the user is sent to the faculty biometric recognition page (fig. 9).

Fig. 4. Biometric Recognition

Fig. 5. Student Successful Biometric Recognition

Fig. 6. Student Answer Sheet Barcode Scanning

Fig. 7. Faculty Biometric Recognition

The faculty biometric recognition page is seen in Figure 9. On this screen, the teacher must first pick a room number, and

then only biometric recognition is enabled; otherwise, the message "Enter Room Number" will be displayed. Following the selection of a room number, biometrics are matched, and the date and time, as well as the room number, are kept in the database. If the biometrics match was unsuccessful for whatever reason, or if the student's information is not in the database, manual input is an alternative. This will be useful in calculating total invigilation duty days in the future.

The time assessment of the proposed system to estimate the time delay during face recognition, fingerprint scanning, and barcode scanning is shown in Table I below.

TABLE I.   PERFORMANCE EVALUATION OF PROPOSED ALGORITHM

Testing	Facial Time (in a sec)	Fingerprint Time (in a sec)	Barcode Time (in a sec)
Test-1	6.65	4.32	2.12
Test-2	7.12	3.76	2.72
Test-3	6.75	4.08	3.12
Test-4	7.98	4.98	2.92

TABLE II.   PERFORMANCE EVALUATION OF PROPOSED ALGORITHM

Testing	Facial	Fingerprint	Both Biometrics
Test-1	Success	Success	Success
Test-2	Success	Success	Success
Test-3	Success	Failure	Success
Test-4	Failure	Failure	Failure

Table II shows the failure and success assessment of the suggested system to estimate the system's accuracy during facial recognition, fingerprint scanning, and barcode scanning. In this table, it can be observed that two out of ten face recognition attempts failed, resulting in an efficiency of 80%. Similarly, for fingerprint recognition, 4/10 failed attempts were reported, resulting in a 60 percent efficiency. When both are combined, just 1/10 of the unsuccessful attempts are detected, and the accuracy observed is therefore 90%. As a result, hybrid biometric recognition is recommended as an accurate attendance authentication technique.

IV. CONCLUSION

The suggested model is an application used to track the attendance of students taking exams. The program will have two main modules: finger-print/facial biometrics and the response sheet's barcode. For student attendance, biometrics are employed, and barcodes are used to record answer books and attendance (RABA) input. The entire system is portable and was built using the Raspberry Pi module. The system yields the following conclusions:

- This framework ensures a quick, painless, and paperless framework that is affordable to the assessment lobby.
- The manual updating and estimating of participation has now been replaced by a superior framework that comprises a robotized cycle of participation coordinated with AI.

- Reduced demand on resources to keep up with physical involvement.
- A simpler and faster inquiry.
- An extremely secure database with no possibility of alteration.

The suggested model would recommend this framework as a replacement for the present approach in schools and colleges. The suggested framework precision and reaction time will be enhanced in future studies.

REFERENCES

[1] Yamamoto KR, Flikkema PG: RFID-based attendance management system for students. 4(2), 1-9, International Journal of Scientific and Engineering Research (2013).

[2] Khatun A, Haque AKMF, Ahmed.S, Rahman MM: Design and implementation of an iris recognition system a computer-based attendance management system International Conference on Electrical Engineering and Information Communication Technology (ICEEICT), Dhaka, 21-23 March, pp. 1–6. (2015).

[3] Panditpautra, Varun: Raspberry Pi-based Biometric Attendance Management System. The International Conference on Advances in Science and Technology (ICAST) will be held for the second time (2019).

[4] Ramirez-Asis, E., Vilchez-Carcamo, J., Thakar, C. M., Phasinam, K., Kassanuk, T., & Naved, M. (2022). A review on role of artificial intelligence in food processing and manufacturing industry. Materials Today: Proceedings, 51, 2462-2465.

[5] Ofualagba Godswill, Omijie Osas, Orobor Anderson, Ibhadode Oseikhuemen, Odicte Etsy: Face Recognition-Based Automated Student Attendance Management System. 5(4), pp. 31-37, International Journal of Educational Research and Information Science (2018).

[6] Dhanalakshmi N., Kumar S., and Sai Y.: Aadhaar-Based Biometric Attendance System Using Wireless Fingerprint Terminals. ieeexplore.ieee.org/iel7.7974917/ 7976734/07976871.pdf (2017).

[7] Poongodi, M., Sharma, A., Hamdi, M., Maode, M., & Chilamkurti, N. (2021). Smart healthcare in smart cities: wireless patient monitoring system using IoT. The Journal of Supercomputing, 77(11), 12230-12255.

[8] H. Rathod, Y. Ware, S. Sane, S. Raulo, V. Pakhare, and I. A. Rizvi: Machine learning-based automated attendance system. ICNTE (International Conference on New Technologies in Engineering), Navi Mumbai, DOI: 10.1109/ ICNTE.2017.7947889, pp. 1-5. (2017).

[9] S. U. Masruroh, A. Fade, and I. R. Julia: Raspberry Pi-based NFC-based Mobile Attendance System with Facial Authorization. 6th International Conference on Cyber and IT Service Management (CITSM), Parapat, Indonesia, pp. 1-6, DOI: 10.1109/CITSM.2018.8674293 (2018).

[10] S. Tamilmani; T. Mohan; S. Jeyalakshmi; Ganesh P. Shukla; Anita Gehlot; Surendra Kumar Shukla "Blockchain Integrated with Industrial IOT Towards Industry 4.0" 27-29 January 2023

IQAC In-charge
Rajiv Gandhi College of Engineering
Karjule Harya, Tal. Parner
Dist. Ahmednagar-414304

958

Principal
R G COE, Karjule Harya.